NASA SOLAR AND HELIOSPHERIC PHYSICS SR&T PROGRAM
CONTRACT NNH07CD05C

Understanding the Relationship between Coronal Mass Ejections and their Interplanetary Counterparts

YEAR 2 SEMI-ANNUAL PROGRESS REPORT

Covering the period 06/28/2008 to 12/27/2008

Submitted by:

Michael Brown-Hayes, Contract Manager
Science Applications International Corporation
10260 Campus Point Drive
San Diego, CA 92121
(SAIC Serial No.: 3188)

Subcontracted to:

Pete Riley, Principal Investigator
Predictive Science, Inc.
9990 Mesa Rim Road, Suite A
San Diego, CA 92121

December 12, 2008

1. Overview

This report summarizes the technical progress made during the first half of the second year of the NASA Solar and Heliospheric Physics SR&T contract "Understanding the Relationship between Coronal Mass Ejections and their Interplanetary Counterparts," (Contract NNH07CD05C) between NASA and Science Applications International Corporation, and covers the period June 28, 2008 through December 27, 2008. Under this contract we have conducted numerical and data analysis related to fundamental issues concerning the relationship between coronal mass ejections and their interplanetary counterparts. During this reporting period, we have: (1) used global MHD simulations to model a specific CME event in detail; and (2) generalized a derivation of MHD conservation relations aimed at inferring the solar properties of CMEs based on in in situ observations of their interplanetary counterparts.

2. Summary of Work

2.1. Modeling the May 12 1997 CME

Global MHD models of Coronal Mass Ejections (CMEs) can provide important insights into the physical processes associated with the eruption and evolution of CMEs and the acceleration of SEPs, and are a valuable tool for interpreting both remote solar and interplanetary in situ observations. Moreover, they represent a virtual laboratory for exploring conditions and regions of space that are not conveniently or currently accessible by spacecraft. The most energetic events typically originate from active regions on the Sun. To accurately model such regions, whilst also capturing the global corona, requires an MHD model that includes energy transport (radiative losses, anisotropic thermal conduction, and coronal heating) in the transition region and corona. Equally importantly, the model must reproduce an accurate ambient solar wind through which the CME propagates. Careful comparison with data from Hinode, STEREO, and SOHO can provide key insights into the mechanisms by which CMEs erupt. In particular, the models should be able to produce emission measurements that can be directly compared with observations.

We have developed a unique treatment of the transition region, allowing us to extend global 3D models of the corona and predict EUV/X-raya emission. This has allowed us to address what the magnetic structure of dimming regions is. We have also explored the importance of shear/energization in CME eruptions, and our results improved when we incorporated sheared fields similar to the observed filament. Specifically: (1) a prominence-like structure was formed which then erupted; and (2) dimmings produced in the simulation compared well with the observations. We also found that the magnetic structure of the dimmings in our simulation is different from the standard model: (1) field lines originating from the dimmings overlie the erupting rope; and (2) eventually, these fields reconnect further as the structure propagates outward.

Comparison with observations also revealed a few shortcomings of the model results. We believe that higher fidelity of the magnetogram structure must be retained for these more detailed comparisons. Armed with this promising first case-study comparison, we have begun to model the May 13, 2005 CME in detail.

The results of this study are summarized in more detail in Appendix A.

2.2. Derivation of Fluid Conservation Relations to Infer Near-Sun Properties of Coronal Mass Ejections from in situ Measurements

Coronal mass ejections (CMEs) are observed both near the Sun using remote solar measurements as well as in the solar wind using in situ measurements. While many relationships have been made between these relatively disparate datasets, a number of connections remain poorly known. As part of this investigation, we used mass, momentum, and energy conservation to derive a set of spherically-symmetric conservation relations based on the observed in situ properties of CMEs and the ambient environment into which they propagate. We focused on fast CMEs that drive a shock and produce a sheath region. These relations allow us to infer the plasma and magnetic field properties of the ejecta close to the Sun based primarily on in situ observations. We considered the limit that both magnetic and thermal plasma pressure could be neglected and derived equations for the initial speed, density, and duration of the ejecta. We then applied these rules to a selection of simulated CMEs (for which the true initial speed could be determined) to verify that the approach is produces relatively reasonable results. In addition, we used the technique to infer the initial speed of an ICME observed in the solar wind. Our estimate compared very favorably with two complementary techniques for estimating the initial speed of CMEs. We plan to pursue these promising results by further generalizing the technique and applying it to more simulated and observed events.

This study, which was initially described in the previous report, has been significantly expanded and generalized. It is described in more detail in Appendix B.

3. Conferences and Publications

During this reporting period, work performed as part of this investigation was presented and/or discussed at the following meetings:

1. Solar Probe Workshop, San Antonio, July, 2008.
2. 37th COSPAR Scientific Assembly, Montreal, Canada, July, 2008.
3. Solar Probe Workshop, Applied Physics Lab., September, 2008.
4. Fall AGU, San Francisco, December, 2008.

The following papers, which relate directly to work undertaken as part of this contract, were either submitted or published during this reporting period:

1. Pete Riley, Jon Linker, Zoran Mikic, and Roberto Lionello, Global MHD Modeling of the Solar Wind and CMEs: Energetic Particle Applications, AIP Conference proceedings, volume 1039, 2008.
2. Pete Riley and David J. McComas, Derivation of Fluid Conservation Relations to Infer Near-Sun Properties of Coronal Mass Ejections from in situ Measurements, Submitted to J. Geophys. Res., 2008.

Additionally, the PI contributed to a number of papers related to the topics of this investigation, and for which he was made a co-author.

4. Future Work

During the next 6 months of this investigation we will continue to develop simulations of specific events. We will complete our analysis of the May 12, 2007 event and begin studying the May 13, 2005 CME, which has been the focus of several working groups, and attempt to relate solar signatures of CMEs with their interplanetary counterparts. We will continue to monitor STEREO observations, and, should a suitable event occur, we will attempt to model it. We have also begun a study to relate in situ measurements of composition with remote solar observations from the UVCS instrument on board SOHO, in an effort to understand the complexity of in situ observations. We will develop this further. Ultimately, we believe that such knowledge will allow us to use composition data as a diagnostic tool for uncovering the mechanism(s) for CME initiation. Finally, we will continue to develop and test our promising new technique for mapping in situ observations back to their solar source.

5. Appendix A

Modeling the May 1997 CME

Jon Linker, Zoran Mikic, Roberto Lionello, Pete Riley, and Viacheslav Titov

Slides from a presentation made at the 37th COSPAR Scientific Assembly, Montreal, Canada.

Understanding Eruptive Phenomena with Thermodynamic MHD Simulations*

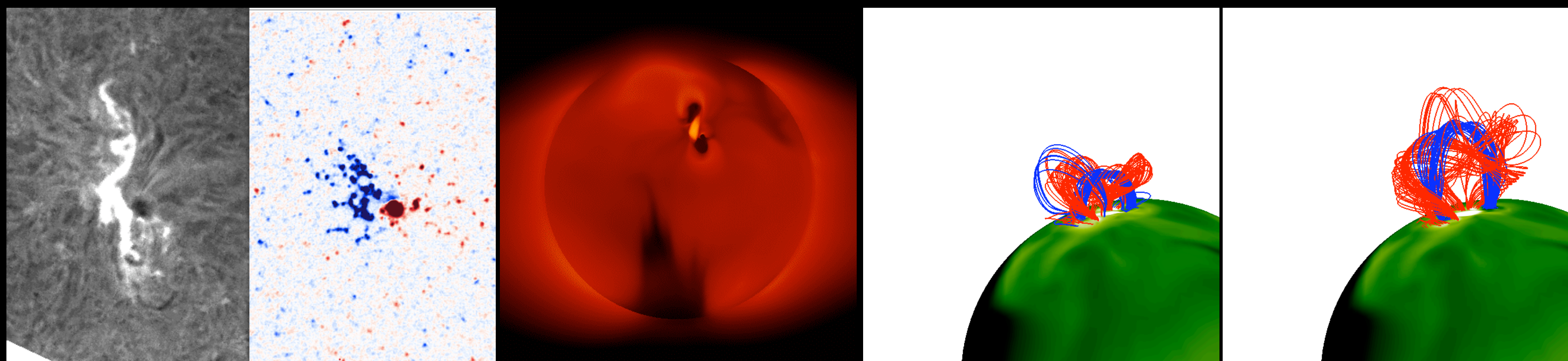

Jon Linker, Zoran Mikic, Roberto Lionello, Pete Riley, and Viacheslav Titov

Science Applications International Corporation

San Diego, California

*Research Supported by NASA and

The Center for Integrated Space Weather Modeling (an NSF STC)

Introduction

- Understanding the structure and dynamics of the solar magnetic field underlies all of the major puzzles in coronal physics.
- Detailed MHD models now exist and are actively applied to many of these questions.
- Data from the Hinode, STEREO, SOHO, and (soon) SDO missions offers the promise of key insights into these problems.
- Discussion/debate often centers upon the interpretation and comparison of modeled magnetic field structure/evolution with features observed in emission.
- For a meaningful comparison, models should be able to produce emission so that they can be *directly* compared with observations.

Introduction (continued)

- Through innovations in the treatment of the transition region, we have been able to extend global 3D models of the corona to predict EUV/X-ray emission.
- I believe that this type of modeling can be used to obtain a deeper understanding of emission features.
- Example: What is the magnetic structure of dimming regions? (2nd part of talk)
- To look at this question, we needed to improve upon the initial simulation results
- The first part of the talk discusses how we obtained a better match to observational features

MHD EQUATIONS
(IMPROVED ENERGY EQUATION MODEL)

$$\nabla \times \mathbf{B} = \frac{4\pi}{c}\,\mathbf{J}$$

$$\nabla \times \mathbf{E} = -\frac{1}{c}\frac{\partial \mathbf{B}}{\partial t}$$

$$\mathbf{E} + \frac{1}{c}\,\mathbf{v} \times \mathbf{B} = \eta\,\mathbf{J}$$

$$\frac{\partial \rho}{\partial t} + \nabla\cdot(\rho\mathbf{v}) = 0$$

$$\rho\left(\frac{\partial \mathbf{v}}{\partial t} + \mathbf{v}\cdot\nabla\,\mathbf{v}\right) = \frac{1}{c}\,\mathbf{J}\times\mathbf{B} - \nabla p - \boxed{\nabla p_w} + \rho\mathbf{g} + \nabla\cdot(\nu\rho\nabla\mathbf{v})$$

$$\frac{\partial p}{\partial t} + \nabla\cdot(p\mathbf{v}) = (\gamma - 1)\left(-p\nabla\cdot\mathbf{v}\ \boxed{-\nabla\cdot\mathbf{q} - n_e n_p Q(T) + H}\right)$$

$$\gamma = 5/3$$

$$\mathbf{q} = -\kappa_{\parallel}\hat{\mathbf{b}}\hat{\mathbf{b}}\cdot\nabla T \qquad \text{(Close to the Sun, } r \lesssim 10R_S\text{)}$$

$$\mathbf{q} = 2\alpha n_e T\,\hat{\mathbf{b}}\hat{\mathbf{b}}\cdot\mathbf{v}/(\gamma - 1) \qquad \text{(Far from the Sun, } r \gtrsim 10R_S\text{)}$$

+ WKB equations for Alfvén wave pressure p_w evolution

May 12, 1997 CME: Comparison of the Simulated Pre-event Corona with Observations

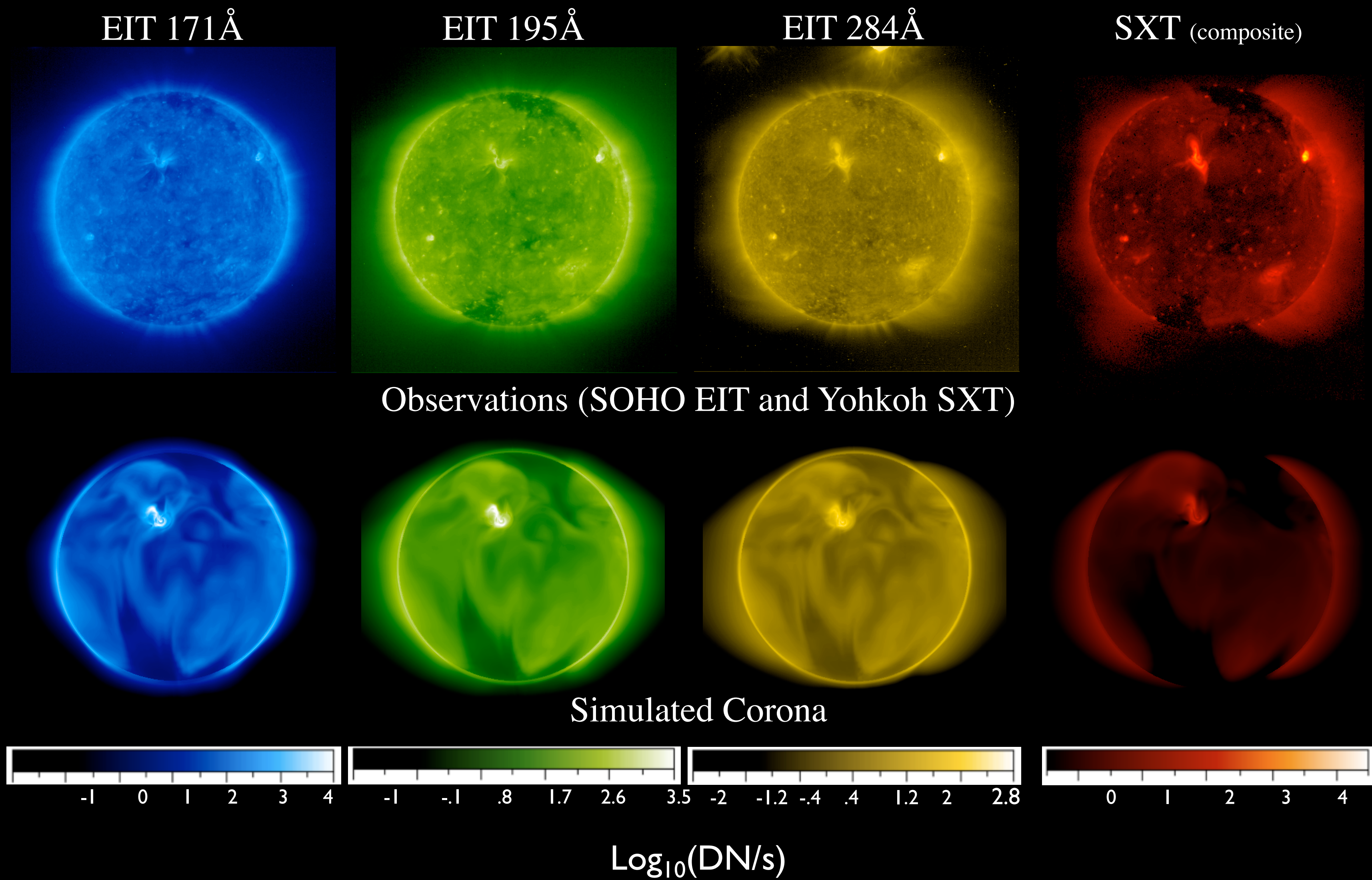

Magnetic Field Evolution in a CME Simulation: CME fluxrope propagates outward from the Sun

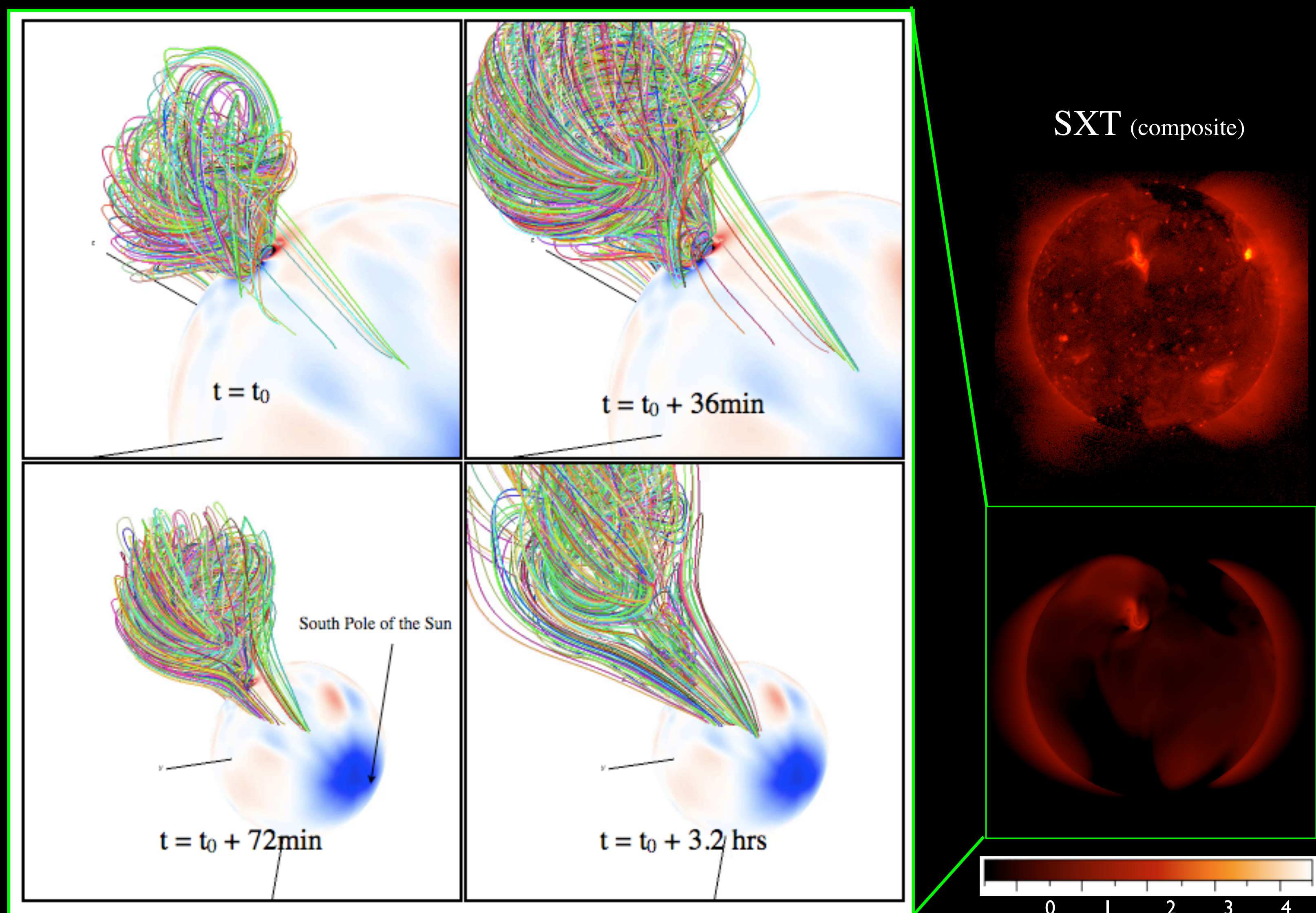

Simulated X-ray emission:
Dimming regions and post-CME loops

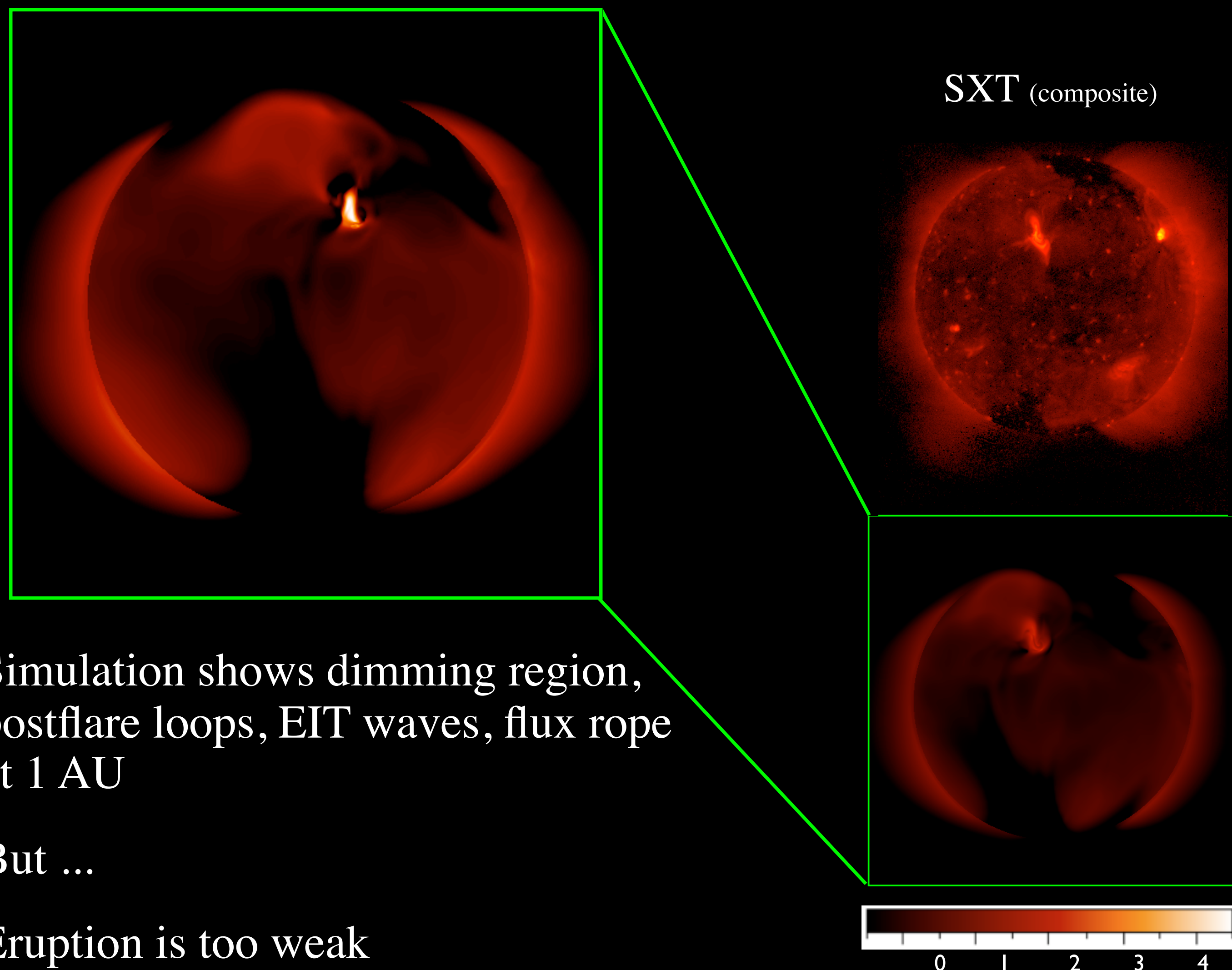

- Simulation shows dimming region, postflare loops, EIT waves, flux rope at 1 AU
- But ...
- Eruption is too weak
- Dimming primarily in the north

Shear Introduced by Flux-Preserving Flows

Global View

Sheared/twisted Field in AR

Vortical flows used for Shear

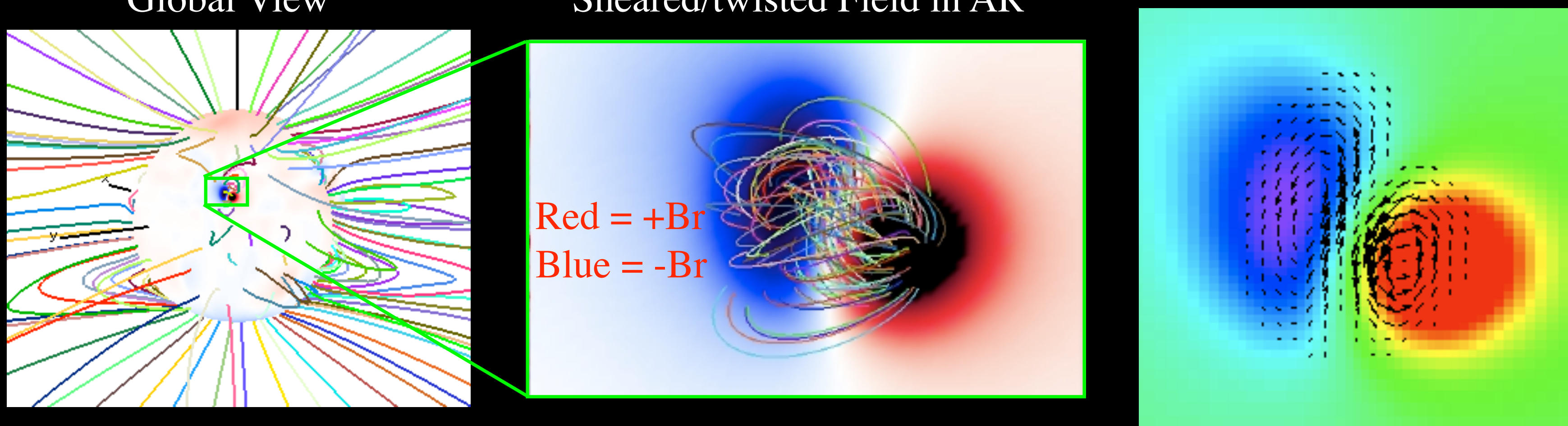

Filament channel & flare (SOON Hα)

NSOKP magnetogram

Smoothed Map

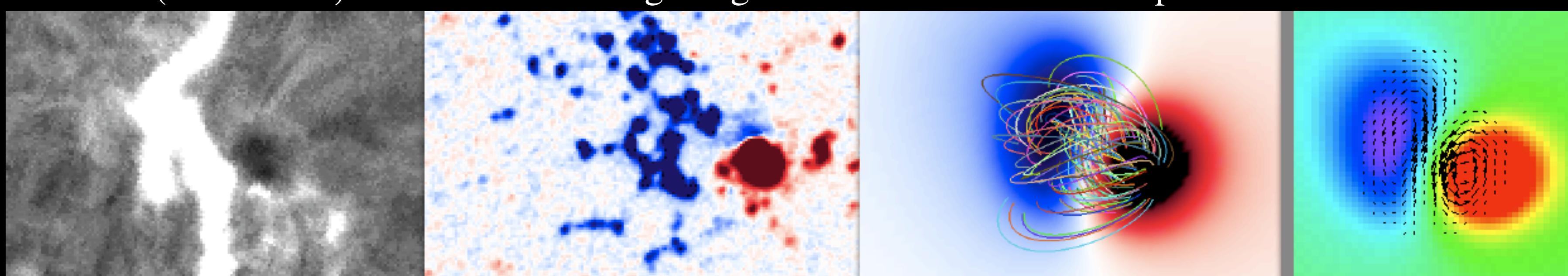

- Shear introduced in the vicinity of large B_r only - not parallel to PIL
- In real case, filament channel (and shear) are much longer and aligned with PIL

Filament Channel & Resulting Eruption

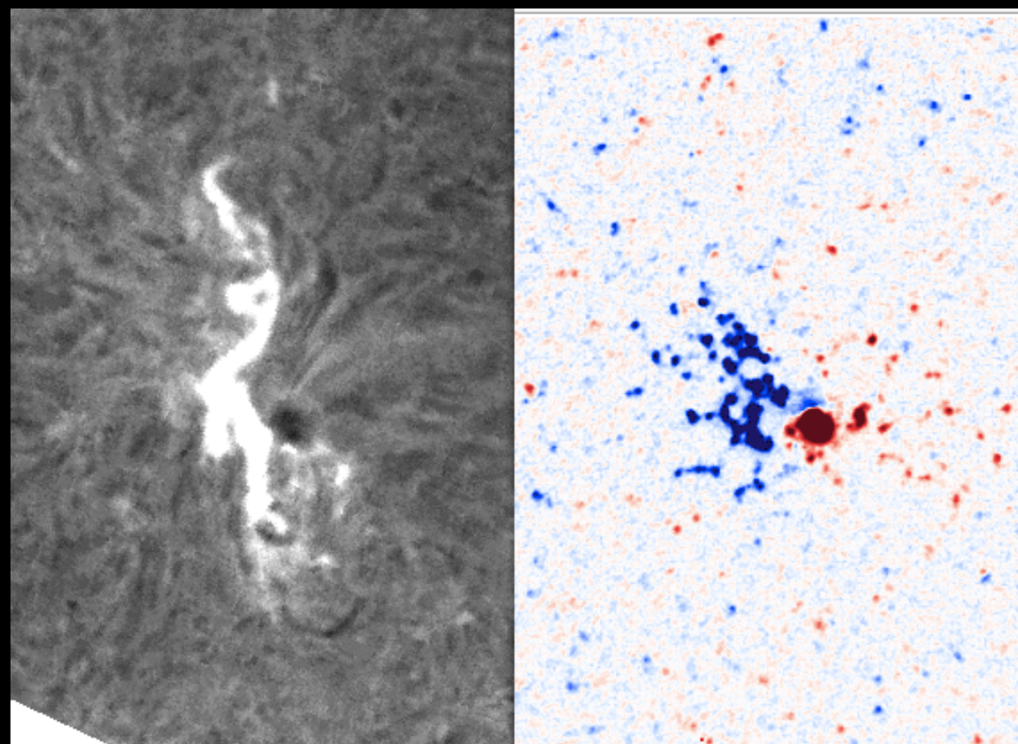

- The filament channel and the resulting flare extend well outside the center of the active region
- Flows in the active region will never create this shear
- How do we deal with this?

Introducing Shear Parallel to the Polarity Inversion Line

- Filament channels have magnetic fields nearly parallel to the polarity inversion line (PIL)
- It is difficult to develop such magnetic fields with flows
- We noticed that in applying our technique for matching vector magnetograms, the algorithm emerged shear along the PIL
- We apply an $\mathbf{E}_{\mathbf{tangential}}$ at the boundary that emerges sheared **B** parallel to the PIL

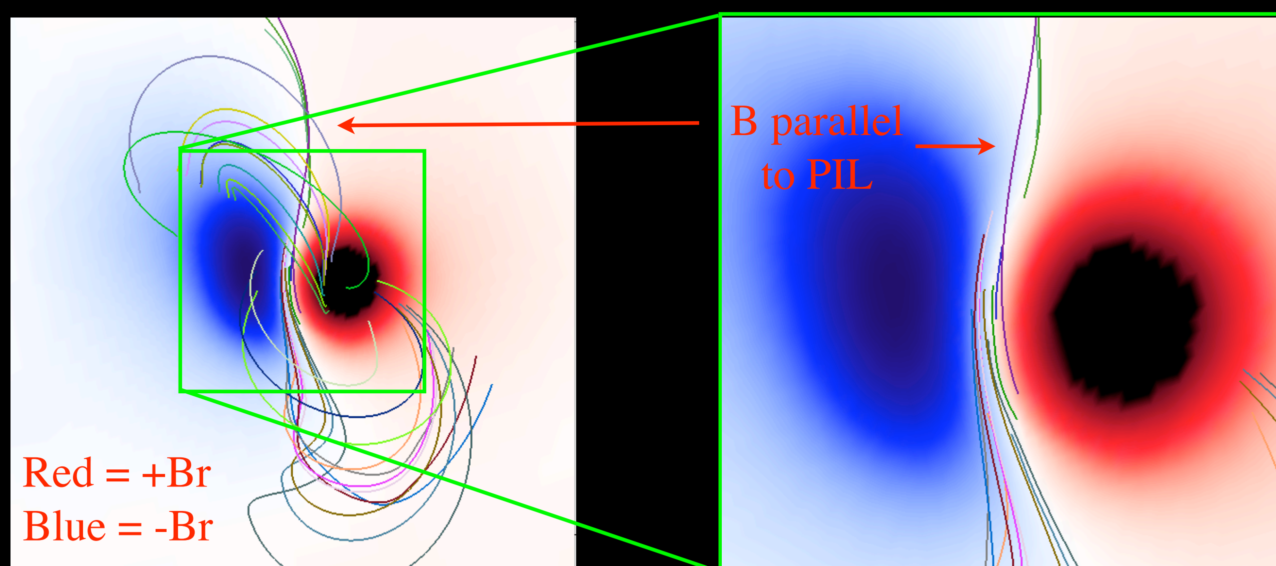

- No flux rope forms (yet)

Converging Flows and Flux Cancellation

- Flux cancellation was observed prior to (and during) the May 12, 1997 CME
- To cancel flux, we apply converging flows perpendicular to the polarity inversion line (PIL)
- Enhanced resistivity is introduced at the PIL at the boundary only (similar to van Ballegooijen et al.)

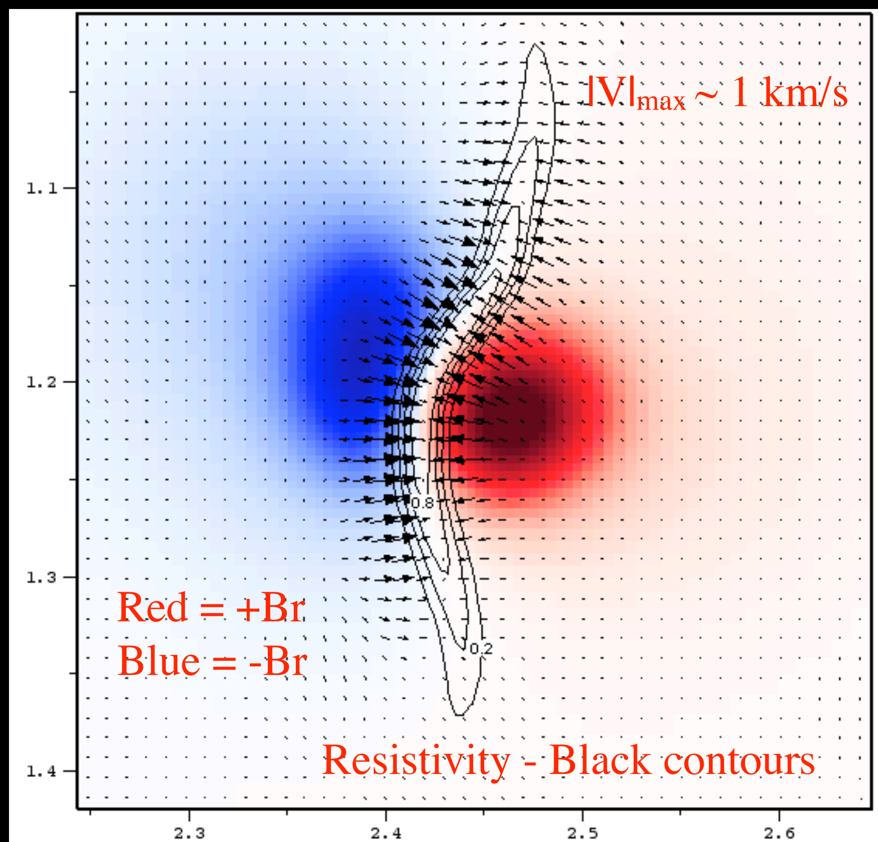

Flux Cancellation Leads to Flux Rope Formation

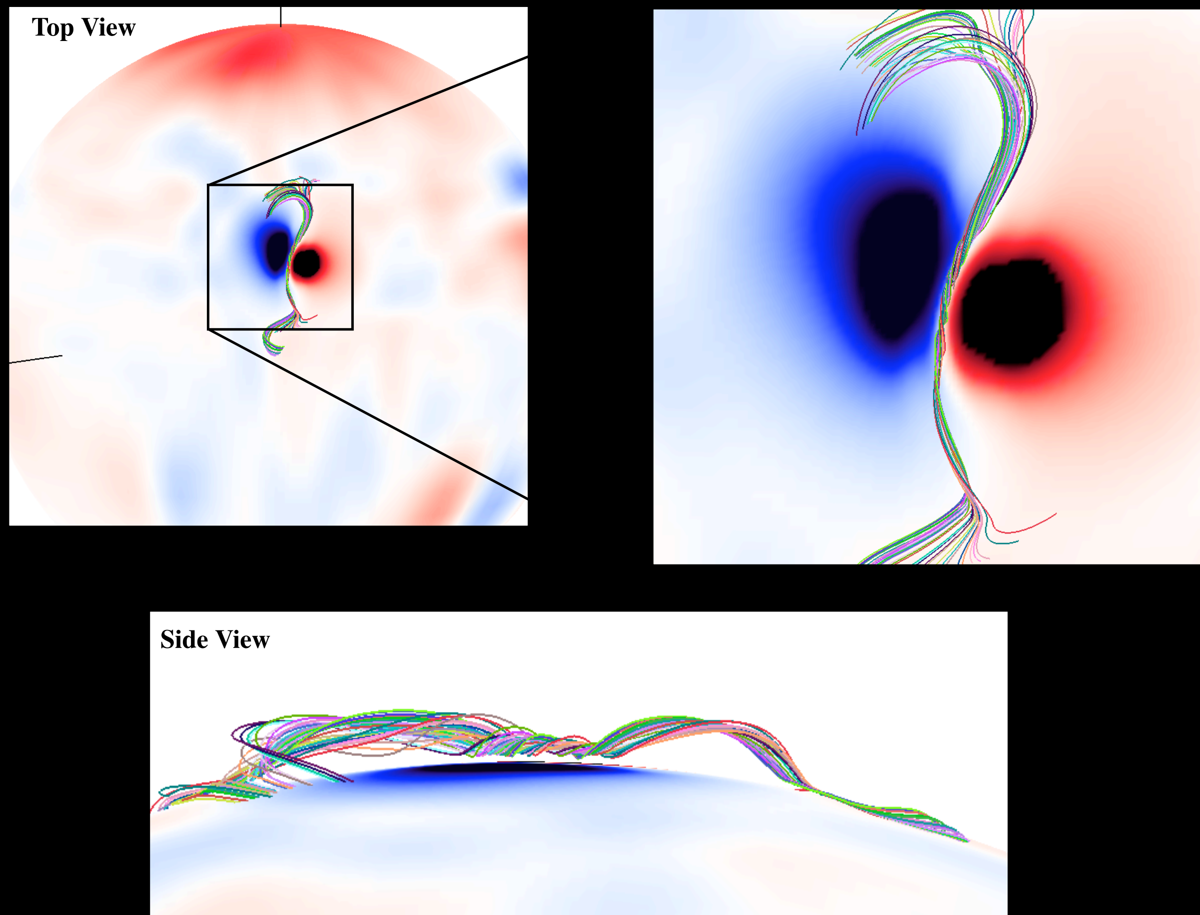

- Prominence-like structure forms along the PIL
- Cold, dense plasma (4×10^4 K, 10^{10} #/cm^3) is lifted into the corona
- With continued cancellation, the structure erupts

Formation of a "Prominence" by Flux Cancellation

- A cut in co-latitude, of Density and Temperature (Eruption starting)

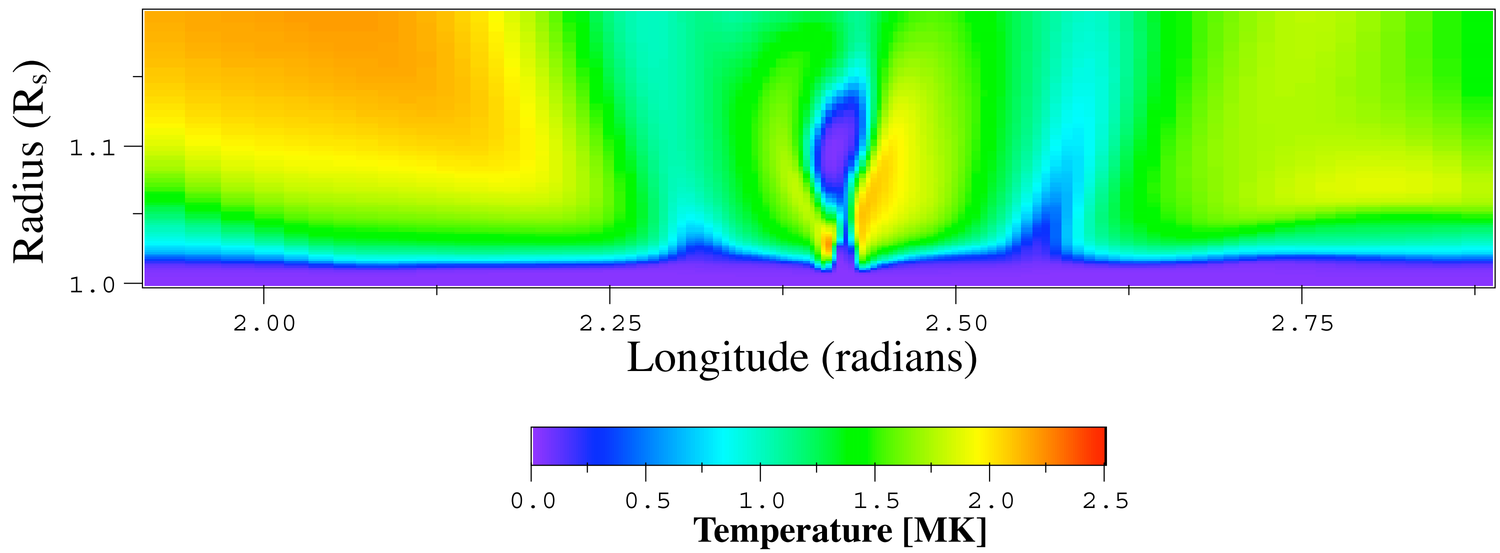

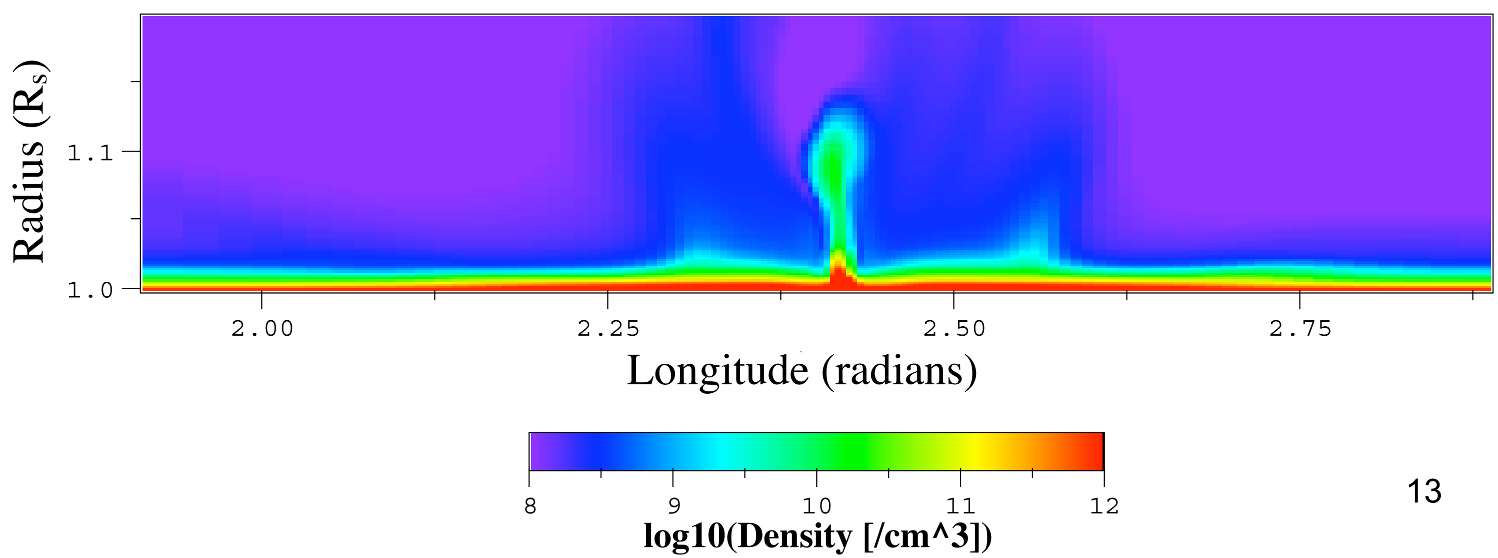

Comparison of Dimming Regions in New Simulation

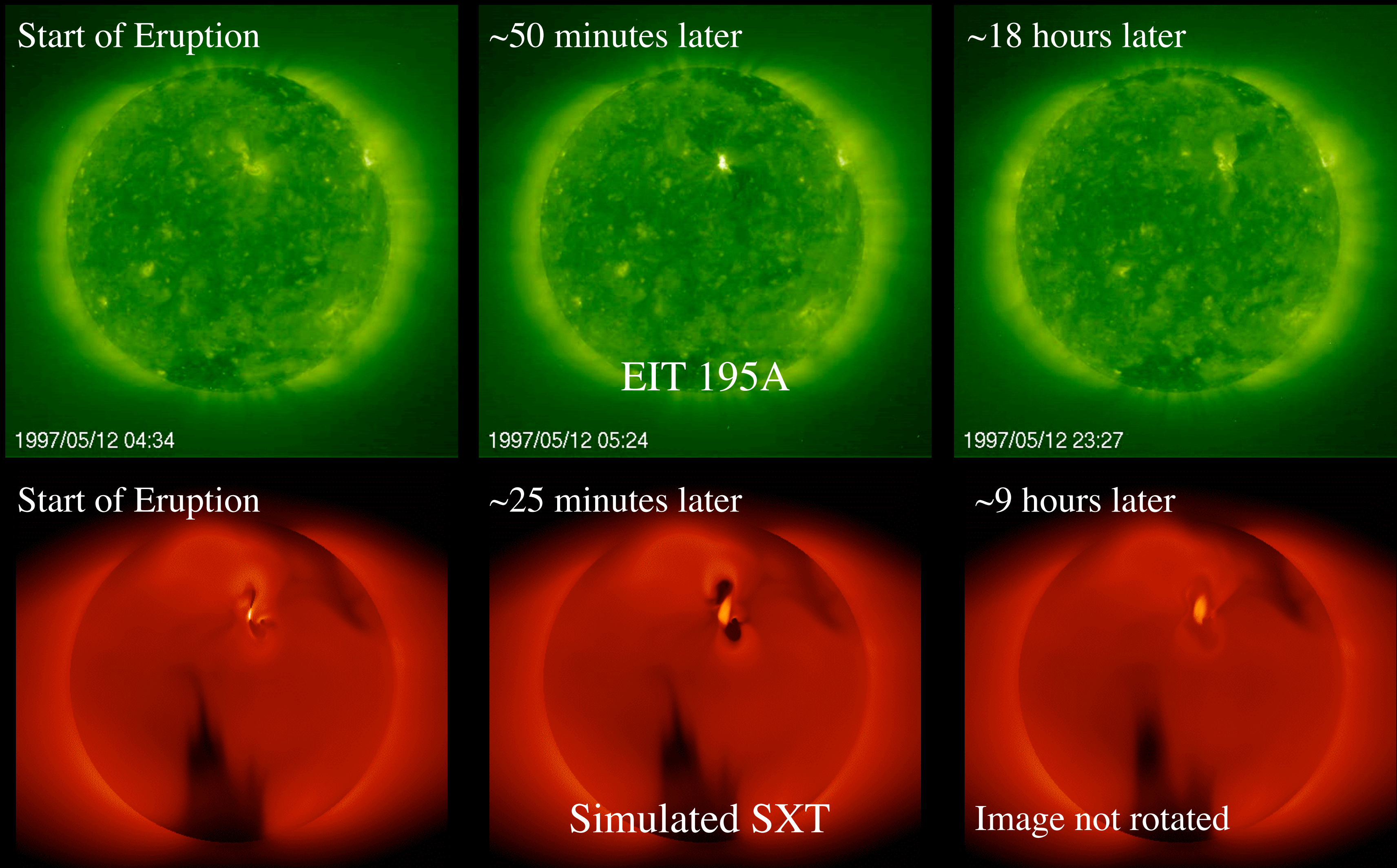

- Both North and South Dimmings now well developed in the simulation
- Shape and location still differs

Analysis of Dimmings - Attrill et al. (2006)

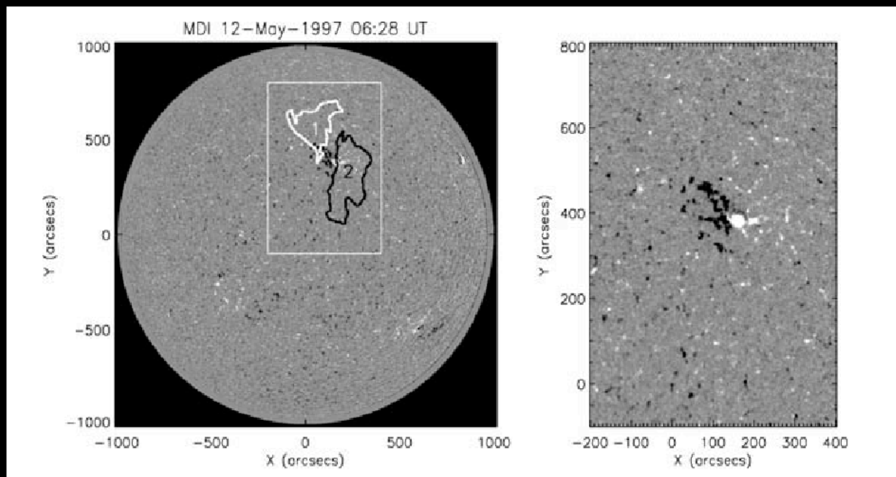

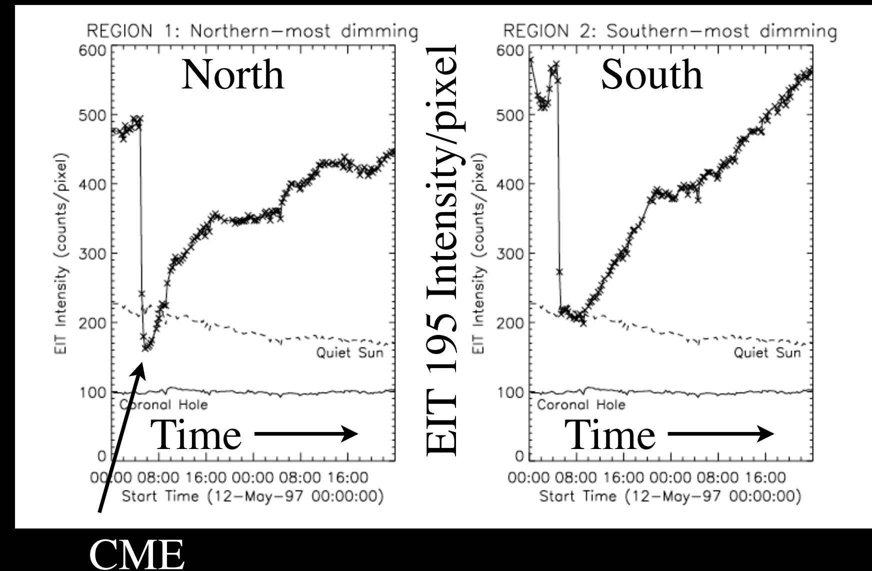

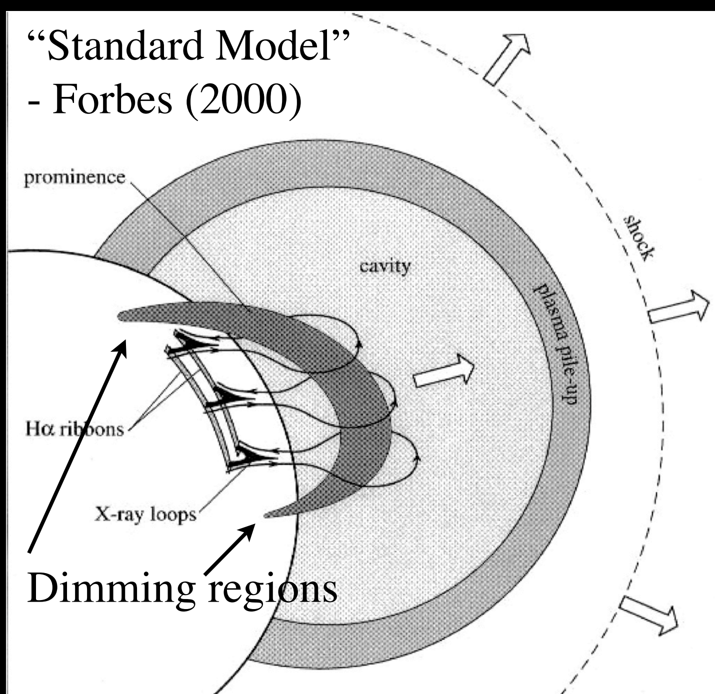

- Computed counts/pixel in dimming regions
- Images differenced from base image prior to eruption
- Dimmings can be seen for ~2 days
- Correlated flux in dimmings with flux in magnetic cloud at 1 AU
- Concluded that cloud was connected to southern dimming

Analysis of Dimming Regions - Simulation

~25 minutes after CME starts

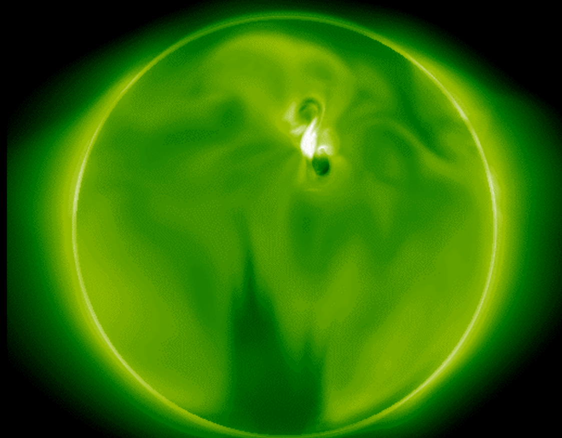

Simulated EIT 195A

~9 hours after CME starts

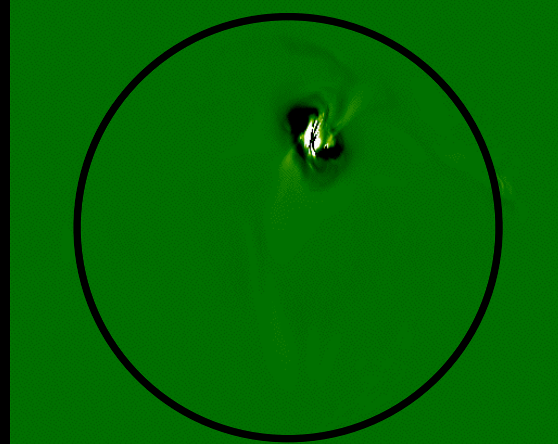

Differenced image - EIT 195A

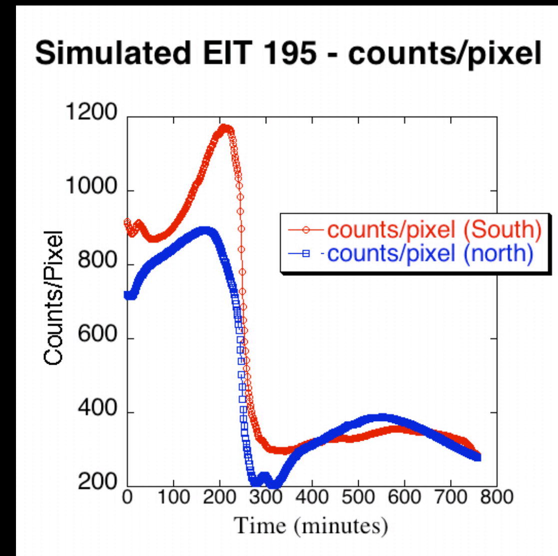

- Dimmings in the simulated images have recovered ~4 hours after CME starts
- Analyzed simulated dimmings in the same way as Attrill et al.
- Dimmings present all 9 hours when analyzed with difference images
- Counts/pixel behavior similar to the observations
- Maximum dimming not exactly co-located with visual image
- What is the magnetic structure of the simulated dimmings?

Trace Magnetic Field Lines from Dimming Locations

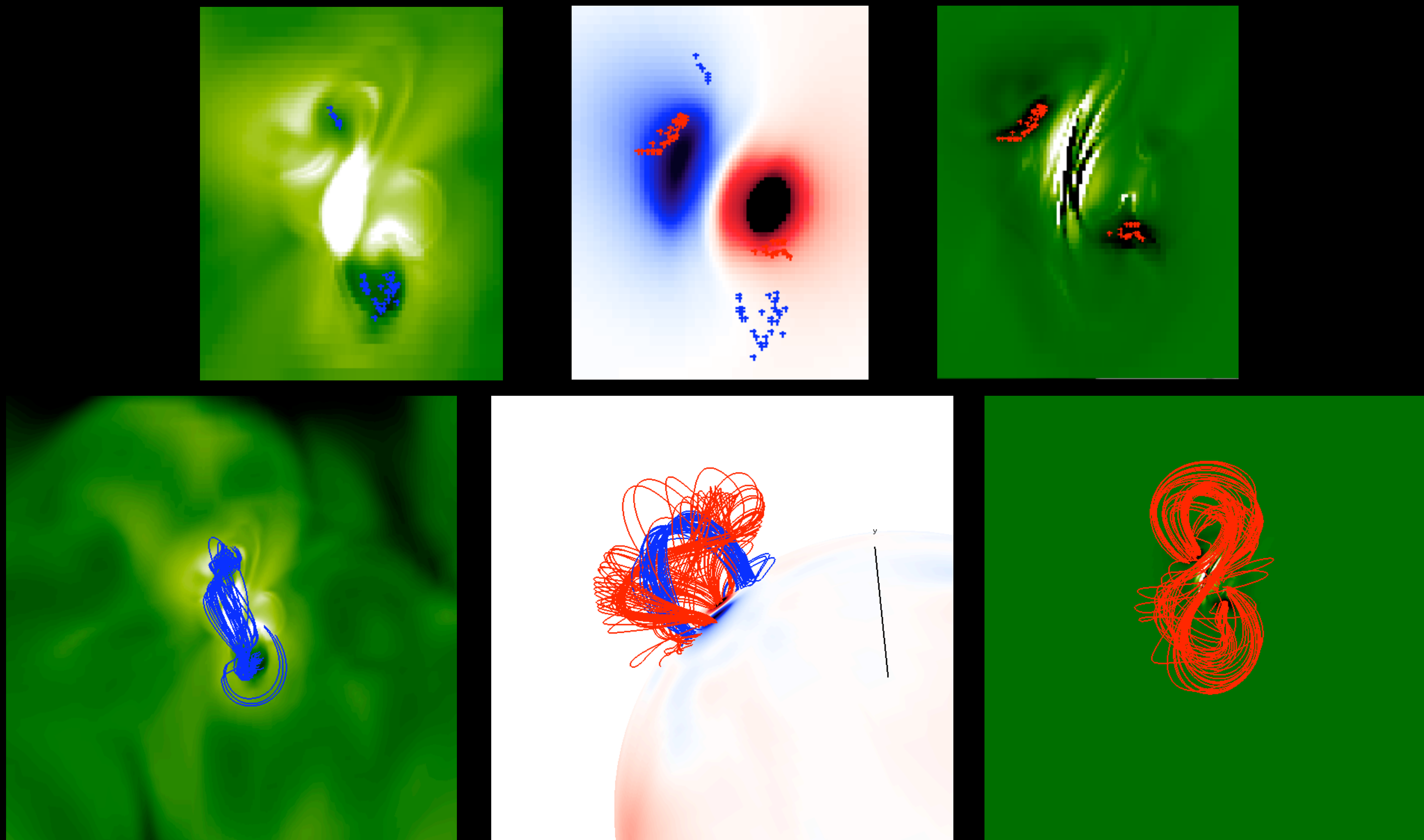

- Blue footpoints - largest dimming from visual inspection
- Red footpoints - largest dimming from subtracting base image

Magnetic Field Lines & Simulated Emission

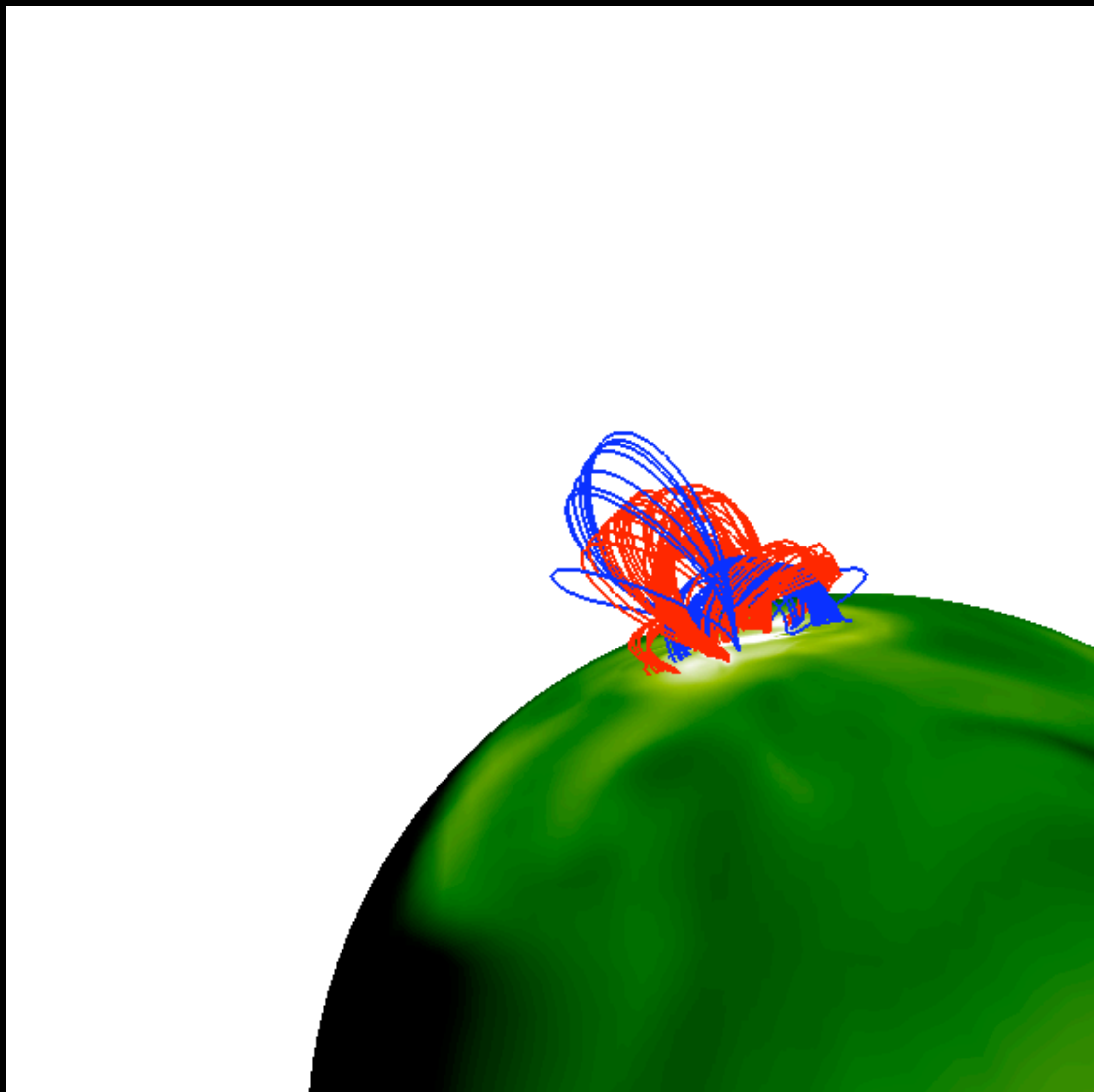

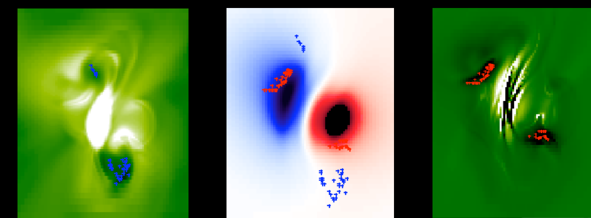

- Blue field lines form the dimmings - but they come from weak flux!
- Red field lines rooted in stronger AR fields
- Blue fields are dragged out by erupting rope
- All fields closed after 9 hours!

Magnetic Field Lines & Simulated Emission

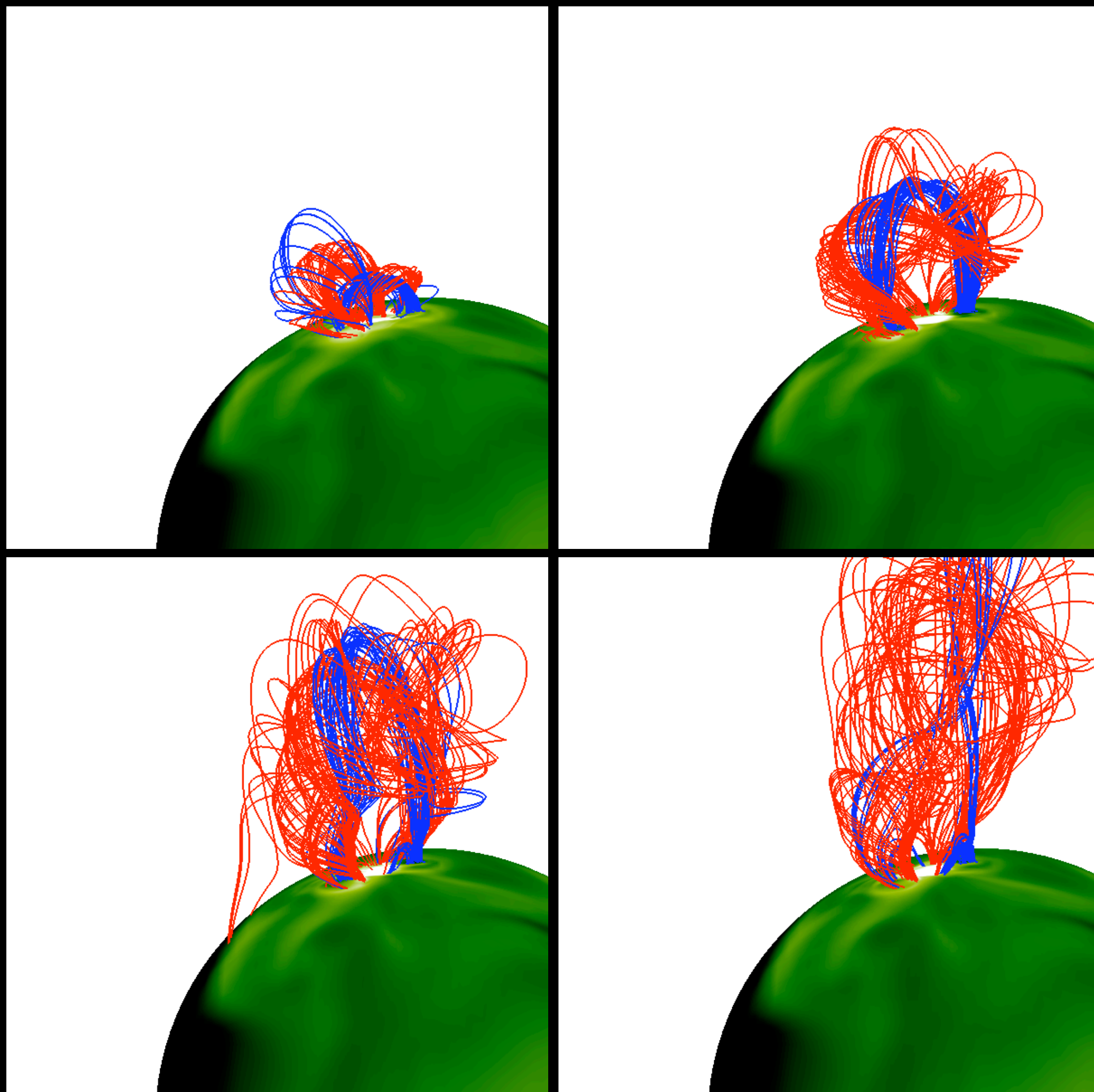

- Not the same as the standard paradigm!
- Caution: Perhaps not directly applicable to May event
- However, real solar fields are even more complicated

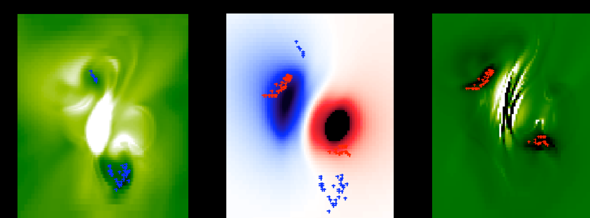

May 2005 CME Simulation: Input Magnetic Data

MDI synoptic magnetic map

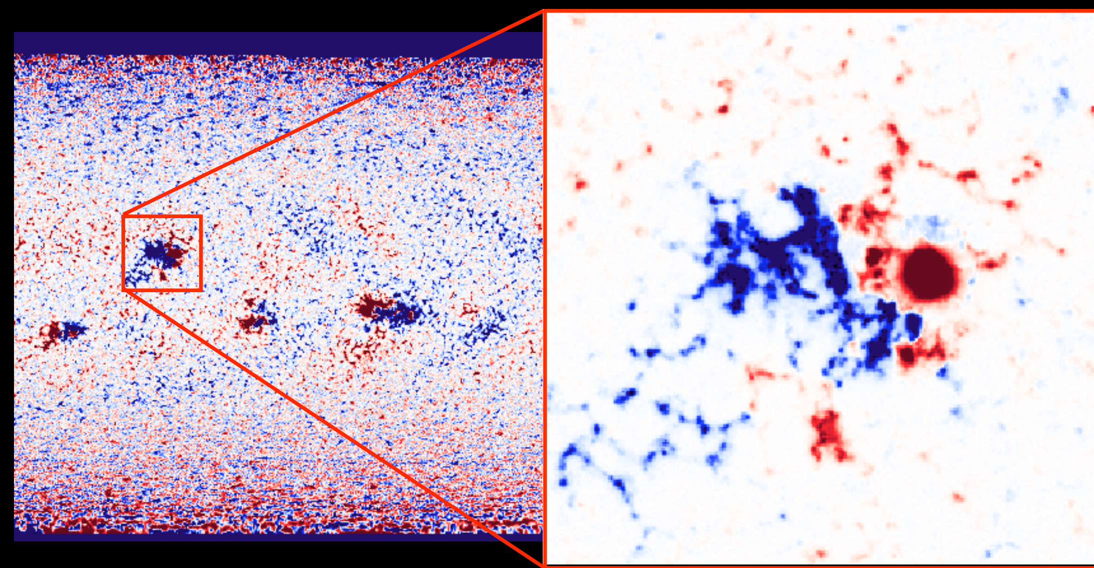

Smoothed version suitable for MHD Calculation.
We are applying less smoothing to the data than in the May 97 case.

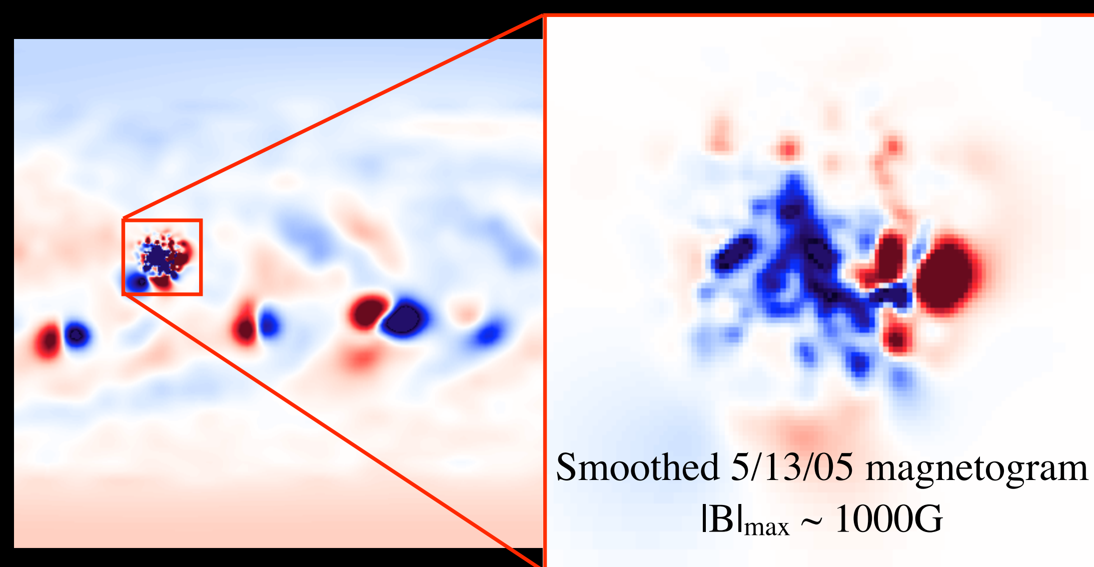

A Preliminary Simulation of the Background Corona

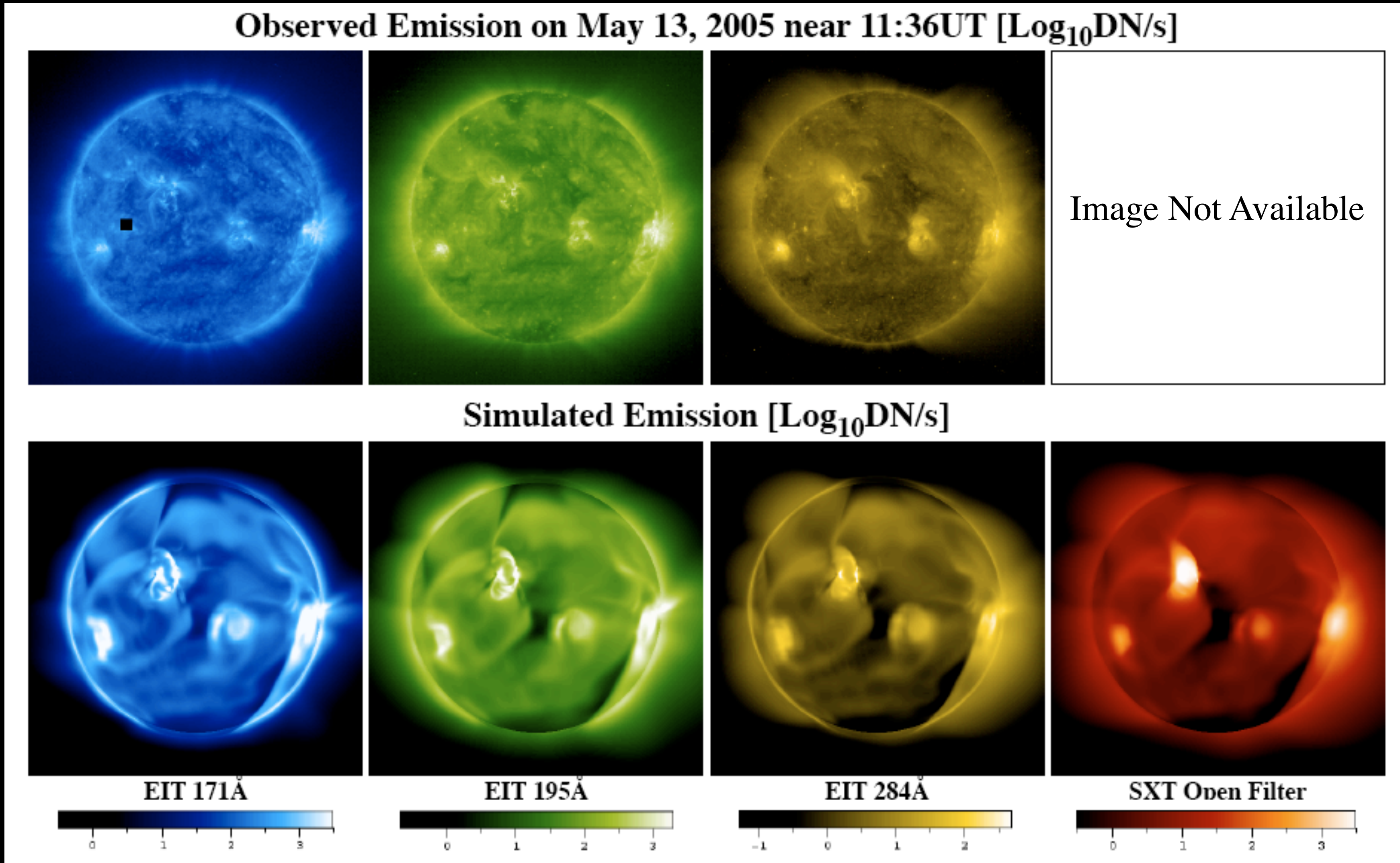

Summary

- MHD thermodynamic simulations can be used to understand what magnetic structures underly observed emission
- The nature of the shear/energization is an important aspect of CME event simulations
    - Results were improved by incorporating sheared field similar to observed filament
    - A prominence-like structure was formed and erupted
    - Dimmings in the simulation are now closer to those observed
    - There are still detailed differences between the simulation and the event

Summary (continued)

- The magnetic structure of the dimmings in the simulation is different than the standard model
  - Field lines originating from the dimmings overlie the erupting flux rope
  - Eventually these fields reconnect further as the structure propagates outward
- Higher fidelity of the magnetogram structure must be retained for more detailed comparisons
- We are attempting this in a new event study:
  The May 13, 2005 CME

6. Appendix B

Derivation of Fluid Conservation Relations to Infer Near-Sun Properties of Coronal Mass Ejections from in situ Measurements

Pete Riley and David J. McComas

Submitted to *J. Geophys. Res.*, December, 2008.

Submitted to J. Geophys. Res.

Derivation of Fluid Conservation Relations to Infer Near-Sun Properties of Coronal Mass Ejections from in situ Measurements

Pete Riley

Science Applications International Corporation, San Diego, CA 92121, USA.

D. J. McComas

Southwest Research Institute, San Antonio, TX 78228, USA.

ABSTRACT

Coronal mass ejections (CMEs) are observed both near the Sun using remote solar measurements as well as in the solar wind using in situ measurements. While many relationships have been made between these relatively disparate datasets, a number of connections remain poorly known. In this study, we use mass, momentum, and energy conservation to derive a set of spherically-symmetric conservation relations based on the observed in situ properties of CMEs and the ambient environment into which they propagate. We focus on fast CMEs that drive a shock and produce a sheath region. These relations allow us to infer the plasma and magnetic field properties of the ejecta close to the Sun based primarily on in situ observations. In this first paper, we consider the limit that both magnetic and thermal plasma pressure can be neglected and derive an equation for the initial speed of the ejecta. We apply this result to: (1) a simulated fast CMEs (for which the true initial speed can is known) to verify that the approach is produces reasonable results; and (2) an observed CME for which several other empirical techniques for inferring initial speed have been applied. Finally, using these results, we derive an estimate for the transit time of a CME from the Sun to 1 AU. Our results are promising, yet tentative. More extensive studies will be necessary to either support or refute this technique.

Subject headings: Sun: coronal mass ejections (CMEs)– Sun: activity–Sun: corona–Sun: magnetic fields–solar wind

1. Introduction

Coronal mass ejections (CMEs) are complex yet spectacular events involving the rapid release of large amounts of solar material, energy, and magnetic field from the Sun and propulsion into interplanetary space. Since they were first clearly identified in space-borne coronagraph images more than 30 years ago (e.g., Tousey (1973); Gosling et al. (1974)), considerable effort has been made to understand their initiation at the Sun and evolution through the solar wind. Over the years, a range of both theoretical and empirical models have been developed to address one or more aspects of the physical processes that are involved with the initiation, eruption, and evolution of a CME as it propagates to Earth. Forbes (2000), Klimchuk (2001), and Lin et al. (2003) have reviewed many of these theoretical models.

White light images record the photospheric radiation scattered by electrons in the ionized coronal plasma, and so they provide a direct diagnostic for the coronal density, which is independent of other physical characteristics of that plasma (such as its temperature). The classic 3-part structure of a CME, observed in white-light images, consists of a bright front, cavity, and core (Figure 2(a)). The bright front is a shell of dense coronal plasma, bounding a darker region and has been interpreted as either (or some combination of) material swept up by the erupting flux rope or pre-existing material in the overlying fields, such as when a streamer erupts (e.g., Wu et al. (1999); Sheeley et al. (1999). The darker region has typically been associated with the presence of a flux rope (e.g. Low (1994)). The innermost bright feature - the so-called core - is also observed to be emitting in the H-alpha line of neutral hydrogen, indicating the presence of much cooler plasma. The inference is that this is prominence material that erupted beneath the field of view of the coronagraph, in conjunction with the CME. This feature has also been proposed as the source of the flux rope as measured in the solar wind (Burlaga 1991; Rust 1994). The basic properties (such as speed and density) for CMEs observed to erupt directly on the limb can be inferred. However, for halo CMEs (that is, CMEs directed toward, or away from the Earth) only the plane-of-sky projected speed can be inferred. Simple geometric models, such as the so-called "cone" model (Zhao et al. 2002) can be used to infer the true speed.

In the solar wind, even classic interplanetary CMEs (ICMEs) have a relatively complicated set of signatures (Figure 2(b)), ranging from counterstreaming suprathermal electrons, low temperature and density, declining speed profile, high and/or variable composition, helium abundance enhancements, field enhancement and low variance, rotation in the magnetic field and low plasma beta (Zurbuchen & Richardson 2006). Few ICMEs have all of these signatures. To compound this, in situ observations (with the notable exception of composition) are a convolution of intrinsic and evolutionary effects: Disentangling them can be difficult, if not impossible. Perhaps the simplest type of ICME is a magnetic cloud (MC) (Burlaga et al. 1981; Klein & Burlaga 1982), which can be identified in the solar wind as low beta plasmas associated with high-field strength flux-rope structures. They are often (but not always) preceded by interplanetary shock waves (Marubashi 1997; Bothmer & Schwenn 1998). The properties of ICMEs, at least along the trajectory of the spacecraft, are well known. However, the limitation of observing the event over such a narrow radial path requires considerable caution when attempting to infer the global (at least transverse) properties of the ejecta. For the case of magnetic clouds, also known as flux ropes, magnetic fitting techniques, such as force-free fitting (Lepping et al. 1990) and the Grad-Shafranov (Hu & Sonnerup 2001) can be used to infer some global properties of the event, subject to the assumptions in the model (force-free configurations and magnetostatic equilibrium, respectively).

The aim of this study is to derive a set of conservation rules that map the properties of CMEs in the solar wind, which are well observed, to their properties near the Sun, which are often poorly determined. We begin by deriving a set of relatively general relationships from mass, momentum, and energy conservation, which retain the thermal and magnetic pressure terms, then simplify the analysis and retain only the dynamic pressure in the momentum equation. This allows us to derive the speed of the ejecta close to the Sun based on measured in situ properties of the event. We apply this result to: (1) a simulated CME; and (2) a CME observed by LASCO/SOHO to assess its validity and accuracy. We then use the expression for the initial speed of the ejecta to compute the transit time of the CME from the Sun to 1 AU. Finally, we conclude by discussing the significant approximations invoked in our analysis and suggest several follow-on studies that could better assess and generalize the techniques presented here.

1.0.1. Derivation of Conservation Relations

We consider the evolution of a spherically-symmetric CME moving away from the Sun from point 1 to point 2. Point 1 is assumed to be within the field of view of a coronagraph, say 20 R_S. Point 2 is assumed to be in the solar wind, where *in situ* measurements are made, say 1-5 AU. We further assume that the CME is traveling significantly faster than the ambient solar wind such that it outruns the plasma behind and ploughs into the plasma ahead. However, point 1 is sufficiently close to the Sun that no appreciable sheath region has developed

The relationship between the CME, ICME, sheath and upstream regions is summarized in Figure 3. The CME near the Sun spans the range denoted by c1. The region upstream, which will become swept-up sheath material is denoted by u1. In the solar wind, the ICME spans the spatial range denoted by c2. The CME's sheath spans the radial distance s2 and the region upstream of the disturbance is denoted by u2. In reality, since the solar wind measurements are being supplied by a spacecraft essentially fixed in inertial space (at least on the timescale it takes for the CME to pass over it), these spatial ranges can be considered as intervals of time. Similarly, near the Sun, although we can describe the CME's properties in terms of radial extent, we will find it simpler to consider timescales taken for the mass to cross a particular boundary, which we will set to $30R_S$ for convenience.

The equation of continuity (mass conservation) can be written in conservative form as as:

$$\frac{\partial \rho}{\partial t} + \nabla \cdot (\rho \mathbf{v}) = 0 \tag{1}$$

where ρ is the mass density of the plasma and $\mathbf{v}$ is the velocity. Similarly, the equation of motion (Momentum conservation) can be written as:

$$\frac{\partial \rho \mathbf{v}}{\partial t} + \nabla \mathbf{T} = 0 \tag{2}$$

where the total stress tensor, $\mathbf{T}$, is:

$$\mathbf{T} = \rho \mathbf{v} \otimes \mathbf{v} - \frac{1}{\mu_o} \mathbf{B} \otimes \mathbf{B} + \left(P + \frac{1}{2\mu_o} B^2 \mathbf{I} \right) - \mathbf{\Pi} \tag{3}$$

and P is the plasma pressure, $\mathbf{B}$ is the magnetic field, $\mathbf{I}$ is the identity matrix, and $\mathbf{\Pi}$ is the viscous stress tensor. For ideal MHD, $\mathbf{\Pi} = 0$. Ohm's law for a ideal medium can also be written in conservative form:

$$\frac{\partial \mathbf{B}}{\partial t} + \nabla \cdot (\mathbf{v} \otimes \mathbf{B} - \mathbf{B} \otimes \mathbf{v}) = 0 \tag{4}$$

where $\mathbf{J}$ is the current density. However, more usually, we write Ohm's law as:

$$\mathbf{E} + \mathbf{v} \times \mathbf{B} = 0 \tag{5}$$

Ampere's Circuital Law is:

$$\nabla \times \mathbf{B} = \mu_0 \mathbf{J} \tag{6}$$

Finally, we can write the energy equation for an adiabatic, IDL MHD fluid as:

$$\frac{\partial}{\partial t}\left\{\frac{\rho v^2}{2}+\frac{P}{(\gamma-1)}+\frac{B^2}{2\mu_0}\right\}+\nabla\cdot\left\{\frac{\rho v^2}{2}\mathbf{v}+\frac{\gamma P}{(\gamma-1)}\mathbf{v}+\frac{\mathbf{E}\times\mathbf{B}}{\mu_0}\right\}=0 \tag{7}$$

Using these conservations equations we will derive some practical relationships between the measured properties of ICMEs in the solar wind and their inferred properties back at the Sun.

We begin by invoking a number of simplifying assumptions. First, consider first the relative contribution of the two terms on the left-hand side of the conservation equations. The first term, $\frac{\partial X}{\partial t}$ represents the rate of change of some quantity, X at a fixed point in space. In general, this will be much less than the spatial change of that quantity in the direction of the flow velocity, $(\mathbf{v}\cdot\nabla)X$, which is contained in the second term. To see this, consider the evolution of an ICME structure at 1 AU. While it is true that the structure has evolved significantly in its passage from the Sun, at 1AU, the spatial variations are much larger than any temporal variations. This assumption likely becomes inaccurate very close to the Sun, where there is significant temporal evolution of the CME over relatively short spatial distances. Second, we assume the plasma flow is radial, i.e., $v_r >> v_\theta, v_\phi$. In the spacecraft frame of reference, and at 1 AU, this is a reasonable assumption. However, it also breaks down very close to the Sun. Third, we retain only radial derivatives (i.e., we assume spherical symmetry). This is clearly an oversimplification; However, at least for events that pass over the spacecraft with a small impact parameter (i.e., the spacecraft traverses through the center of the ejecta), it is likely to be a reasonable first approximation. Thus, for some vector $\mathbf{A}$:

$$\nabla\cdot\mathbf{A}=\frac{1}{r^2}\frac{\partial}{\partial r}\left(r^2 A_r\right) \tag{8}$$

With these assumptions, the mass continuity equation (Equation (1)) simplifies to:

$$\frac{\partial}{\partial r}\left(r^2\rho v_r\right)=0 \tag{9}$$

Similarly, it can be shown that the radial divergence of the total stress tensor in spherical coordinates reduces to:

$$(\nabla\cdot\mathbf{T})_r=\frac{1}{r^2}\frac{\partial}{\partial r}\left(r^2 T_{rr}\right)-\frac{T_{\theta\theta}+T_{\phi\phi}}{r} \tag{10}$$

Finally, using Ohm's law (equation 5), the energy equation reduces to:

$$\frac{\partial}{\partial r}\left\{r^2 v_r\left(\frac{\rho v_r^2}{2}+\frac{\gamma P}{\gamma-1}+\frac{B_t^2}{\mu_0}\right)\right\}=0 \tag{11}$$

where the field transverse to the radial direction, $B_t^2 = B_\theta^2 + B_\phi^2$.

We supplement these equations with the following polytropic relationship:

$$\frac{d}{dt}\left(\frac{P}{\rho^\gamma}\right)=0 \tag{12}$$

where d/dt is the convective derivative. With the aforementioned approximations, this reduces to:

$$v_r\frac{\partial}{\partial r}\left(\frac{P}{\rho^\gamma}\right)=0 \tag{13}$$

We note that while mass and energy conservation and the polytropic relationship can be cast in the form: $\frac{\partial X}{\partial r} = 0$, the momentum equation cannot, making it more difficult to apply directly. However, these equations are not independent. In particular, combining the equation of state with the continuity equation leads to the energy equation.

In reality, *in situ* spacecraft measure the properties of an ICME as it flows over it. Thus we cannot integrate directly over the elemental distance dr. Instead, we must integrate over time, dt at the heliocentric distance of the spacecraft.

Equation (9) can be used to relate the properties of the CME near the Sun (say at $r = r_1 = 10R_S$) to the properties of the ICME (say at $r = r_2 = 1\mathrm{AU}$). Assuming that the speed and duration of the CME at r_1 are known, we can estimate the average density at r_1:

$$\rho_{c1}=\frac{r_{c2}^2 I_1}{r_{c1}^2 v_{c1}\Delta t_{c1}} \tag{14}$$

where the subscripts 'c' refer to CME and '1' and '2' refer to the locations near to and far from the Sun and we have assumed that the density and speed within the CME near the Sun are approximately constant. For simplicity, we have also removed the subscript 'r' in the velocity component. From this point forward, $v = v_r$ and $B^2 = B_t^2$. We have also defined the known quantity I_1 as:

$$I_1=\int_{c2}\rho v_r dt \tag{15}$$

The quantity I_1 is the time integral of the mass flux of the ICME along the trajectory of the spacecraft. Thus it can be interpreted as the total "mass" per unit area of the ICME.

We can repeat this procedure for the sheath region of the ICME. To relate this to the near-Sun environment, we assume that close to the Sun, no sheath region exists. However, there is a region upstream of ejecta close to the Sun that will be swept up to become sheath material. Applying mass conservation to these regions allows us to deduce the duration of the upstream region near the Sun (which will appear in subsequent equations and can be substituted for):

$$\Delta t_{u1} = \frac{I_2}{\rho_{u2} v_{u2}} \tag{16}$$

Again, we have defined the known quantity:

$$I_2 = \int\limits_{s2} \rho v_r dt \tag{17}$$

which is integrated over the sheath region of the ICME, and again, represents the "mass" of the ICME sheath region per unit area. Note that we have also made use of the fact that we can estimate the density and speed of the region upstream of the CME near the Sun from the values of the plasma upstream of the sheath region of the ICME. Specifically, we assume that $v_{u1} = v_{u2}$ and $\rho_{u1} = (r_{u1}/r_{u2})^2 \rho_{u2}$.

Intuitively, it makes sense that, for a fast CME, we can approximate momentum flux balance by considering only the (I)CME and upstream regions. The CME is outrunning the ambient solar wind behind it, creating a rarefaction wave, the effect of which is to accelerate slower ambient plasma and decelerate the CME plasma at the trailing edge. However, this is a small effect in terms of the dynamics of the ICME. At the leading edge of the ICME, as it ploughs into the ambient solar wind ahead, it accelerates, compresses, and heats the plasma. These effects persist upstream as far as the location of the shock. By definition, no momentum transfer occurs beyond this boundary.

Finally, using the previous relationships, energy conservation for the combined CME and sheath regions can be shown to be:

$$r_{c1}^2 \Delta t_{c1} v_{c1} \left(\frac{\rho_{c1} v_{c1}^2}{2} + \frac{\gamma P_{c1}}{\gamma - 1} + \frac{B_{c1}^2}{\mu_0} \right) + r_{u1}^2 \Delta t_{u1} \left(\rho_{u2} \left(\frac{r_{u2}}{r_{u1}} \right)^2 \frac{v_{u2}^2}{2} + \left(\frac{r_{u2}}{r_{u1}} \right)^{10/3} \frac{\gamma P_{u2}}{\gamma - 1} + \left(\frac{r_{u2}}{r_{u1}} \right) \frac{B_{u2}^2}{\mu_0} \right) = I_3 \tag{18}$$

where:

$$I_3 = \int\limits_{c2+s2} r^2 v_r \left(\frac{\rho v_r^2}{2} + \frac{\gamma P}{\gamma - 1} + \frac{B_t^2}{\mu_0} \right) dt \tag{19}$$

The parameter I_3 represents the scaled energy per unit area, along the trajectory of the spacecraft. Since I_1, I_2, I_3, and all quantities with a '2' subscript can be computed from *insitu* observations, equations (13), 14), 16), and 18) represent 4 relationships with 6 unknowns. Thus, if, for example, we could estimate v_{c1} and Δt_{c1} from coronagraph observations, we could solve for ρ_{c1}, Δt_{u1}, P_{c1}, and B_{c1}. Of particular scientific relevance, are the values for P_{c1}, and B_{c1}, or the plasma $\beta = 2mu_0 P_{c1}/B_{c1}^2$, which would allow us to infer the relative contributions of thermal and magnetic pressure to the initial expansion of the ejecta close to the Sun; a quantity that is not well known (Gosling et al. 1994), but one that could provide important constraints on models of CME eruption and/or early evolution.

1.0.2. Simplification of Conservation Relations to include only Dynamic Pressure

In the previous section, we derived general equations to solve for ρ_{c1}, Δt_{u1}, P_{c1}, and B_{c1} under the assumption that we could infer v_{c1} from observations. However, for Earth directed CMEs (the so-called "halo" CMEs) only the projected plane-of-sky speed can be directly computed from the observations. Geometric models, such as the "cone" model (Zhao et al. 2002) can be used to infer the true velocity. Reiner et al. (2007) have also developed a technique to infer the initial CME speed from: (1) low-frequency radio emissions from the CME-driven shock; (2) the transit time to 1 AU; and (3) inferred *in situ* shock speed. However, it is difficult to assess the accuracy of these techniques since no reliable independent estimate can be made. Moreover, we have found (Riley and McComas, unpublished manuscript, 2008) that these two approaches generally do not agree well. To address this important issue, we can solve for v_{c1} by further simplifying the conservation relations, assuming that the thermal plasma and magnetic pressures are negligible, relative to the dynamic pressure.

To assess the validity of neglecting the thermal plasma and magnetic pressure terms in the momentum equation, we can compare their relative contributions to the total momentum flux at 1 AU and then, by extrapolation, map these values back toward the Sun. Assuming typical solar wind values at 1 AU for number density ($n = 5 \times 10^6 m^{-3}$), speed ($v = 500 \times 10^3 m^3$), we derive a dynamic pressure, ρv^2 of $\sim 2 \times 10^{-7}$ Pa. Assuming a typical transverse magnetic field value of $B \sim 5 \times 10^{-9}$T yields a magnetic pressure of $\sim 10^{-11}$ Pa. Finally, assuming a typical proton temperature, $T_p \sim 5 \times 10^4$ K, yields a thermal pressure of $\sim 3.5 \times 10^{-12}$ Pa. Thus the ratio of the dynamic pressure to magnetic pressure is $\sim 10^{-4}$ and the ratio of the dynamic pressure to thermal pressure is 10^{-5}. Clearly, in the solar wind, their neglect is justified.

Closer to the Sun, however, the density, temperature, and magnetic field all increase. Limiting our closest distance to say $20R_S$, we can assume that v_r remains constant and that the other parameters vary due to spherical geometry of the expanding solar wind. Thus density increases as r^2, the transverse magnetic field increases as r, and the pressure increases as $r^{10/3}$. To a first approximation then, the ratio of the dynamic pressure to the magnetic pressure remains constant and the ratio of the dynamic pressure to the thermal pressure increases as $r^{4/3}$. Even at $10R_S$, this ratio increases by only $(215/10)^{4/3} \sim 60$. Given that this ratio at 1 AU was 10^{-5}, we are justified in neglecting their contribution near the Sun.

Thus, neglecting the thermal and magnetic terms in the energy equation, equation (18) simplifies to:

$$r_1^2 \Delta t_{c1} n_{c1} v_{c1}^3 + r_2^2 \Delta t_{u1} n_{u2} v_{u2}^3 = r_2^2 \Delta t_{c2} n_{c2} v_{c2}^3 + r_2^2 \Delta t_{s2} n_{s2} v_{s2}^3 \tag{20}$$

where we have broken the right-hand side into the ICME and sheath terms, approximated the integrals with average values, and replaced the mass density, ρ, with number density, n.

We can approximate the equations for mass conservation within the ICME and sheath region as:

$$r_{c1}^2 n_{c1} v_{c1} \Delta t_{c1} = r_{c2}^2 n_{c2} v_{c2} \Delta t_{c2} \tag{21}$$

and

$$n_{u2} v_{u2} \Delta t_{u1} = n_{s2} v_{s2} \Delta t_{s2} \tag{22}$$

Thus we now have 3 equations and 12 variables. Of these, only 3 are unknown. Equation (21) allows us to substitute $n_{c1}\Delta t_{c1}$ for known quantities in the ICME in equation (20), while equation (22) allows us to substitute Δt_{u1} for known quantities in the sheath region and upstream of the ICME. After some simple algebra, we arrive at:

$$v_{c1} = \sqrt{v_{c2}^2 + \frac{\Delta t_{s2}}{\Delta t_{c2}} \frac{n_{s2}}{n_{c2}} \frac{v_{s2}}{v_{c2}} \left(v_{s2}^2 - v_{u2}^2\right)} \tag{23}$$

This expression can be interpreted heuristically in the following way. First, the initial speed, v_{c1}, depends on the measured speed in the solar wind, v_{c2}, that is, the first term under the square root. This speed is then boosted by a term that depends on the ratio of: (1) the duration of the sheath region to the ICME region; (2) the density of the sheath to the ICME; and (3) the velocity of the sheath relative to the ICME. Intuitively, it makes sense that a faster initial CME would produce larger values in all 3 of these ratios. Finally, the second term under the square root depends on the difference of the squares of the sheath to upstream solar wind speed. Again, the larger this value, the larger would be the initial CME speed. We can also consider a few simple limits to explore this relationship further. For example, if there were no sheath, then $\Delta t_{s2} = 0$ and $v_{c1} = v_{c2}$. Similarly, if the speed of the sheath region matched that of the upstream region, there would effectively be no sheath and again, $v_{c1} = v_{c2}$.

The CME boundary in the context of our analysis is the mass boundary, that is, the boundary of the ejected plasma. This may (and often is) different from boundaries derived based on other parameters, particularly counterstreaming suprathermal electrons, as well as rotations in the magnetic field. In practice, all relevant ICME parameters are scrutinized to best assess where the boundaries lie; however, depending on the nature of the study being performed, preference is often given to a sub-set of these signatures. In order to estimate the best value for v_{c1}, it is crucial that we identify the mass boundaries of the ejecta as accurately as possible, since they modify the terms on the right-hand side of equation (23) in two ways: (1) the ratio of the duration of the sheath to ICME intervals; and (2) the average properties of speed and density within these regions.

Finally, it is worth emphasizing that equation (23) does not depend on distance from the Sun, r. This is not an evolutionary equation, but rather approximates mass and energy balance, assuming that at the initial state, no sheath region exists. Thus it cannot be applied to infer the ICME speed at some arbitrary distance from the Sun, based on measurements made further out.

2. A Numerical Test using a 1-D Hydrodynamic Model

Our derivation can be tested using a simplified one-dimensional, hydrodynamic model of CME evolution in the solar wind (Riley & Gosling 1998; Riley et al. 2001). The model is particularly appropriate for assessing the accuracy of equation (23) because it assumes that magnetic effects are negligible (although thermal pressure effects remain) and that the evolution is spherically symmetric. Figure 4 summarizes one specific case, where we launched a crude CME from an inner boundary located at 0.14 AU. The "CME" consisted of a step increase in speed of 700 km/s, coincident with a $\times 10$ increase in density. These particular profiles were chosen so as to mimic a CME whos initial speed was considerably larger than the ambient solar wind (700 km/s in this case, a factor of two increase) and whos density was considerably larger, thus providing sufficient internal pressure so as not to collapse and, more importantly, a sufficiently large momentum flux to generate a substantial sheath region. The boundaries of the ejecta and the location of the shock front at each location (0.14, 0.5, 1.0, 1.5, and 2.0 AU) are marked by solid and dashed lines of the appropriate color, respectively. Using these regions, we can compute the various terms present on the right hand side of equation (23) for the 4 locations beyond the boundary. The final row shows v_{c1} as computed from equation (23) for data at the 4 distances These estimates can be compared with the "true" value for v_{c1}, which was 1400 km/s.

3. A Case Study

For the purposes of illustrating the application of equation (23) to observed events, we have chosen the November 22, 2001 CME. This event is, in as much as is possible, an ideal event for studying momentum transfer between CMEs and ambient solar wind. The solar wind was otherwise very quiescent during this period. The ICME drove a strong shock ahead of it and generated a substantial sheath region. The speed differential between ICME and upstream solar wind was $\sim$ 400km/s at 1 AU. The ejecta itself contained a well-defined flux rope, which aided in the identification of the sheath and ICME boundaries. These boundaries were relatively easy to identify. The event is summarized in Figure 5. We estimated the following values for the parameters needed to compute v_{c1} in equation (23): $v_{c2} = 800$ km/s; $v_{s2} = 900$ km/s; $v_{u2} = 450$ km/s; $n_{s2} = 24.1$ cm^{-3}; $n_{c2} = 2.0$ cm^{-3}; $\Delta t_{s2} = 1.5$ days; and $\Delta t_{c2} = 3.3$ days. With these values, we deduce that $v_c1 = 2152$ km/s. (Table 1 summarizes all of the relevant parameters). This can be compared with the value obtained from low-frequency radio emissions and transit times (Reiner et al. 2007) of 2250 km/s as well as the value derived from a "cone" model (Xue et al. 2005) of 2519 km/s.

4. CME Transit Times

The transit time of a CME to 1 AU (τ) is defined as the time between the first observation of the CME by a coronagraph, and the arrival of the leading edge of the ICME at 1 AU (Owens & Cargill 2004). This is approximately equivalent to the time it takes the CME to travel from region 1 to region 2 (if that is where the in situ observations are made) in our analysis, since region 1 is defined as sufficiently close to the Sun such that no appreciable sheath has yet developed. Since we measure v_{c2} and estimate v_{c1}, we can compute τ provided we know the deceleration profile of the (I)CME. In theory, there are an almost limitless number of deceleration profiles that would take v_{c2} down to v_{c1} during its outward propagation to 1 AU. For example, Vršnak & Gopalswamy (2002) derived an equation of motion for the ICME assuming that aerodynamic drag was the only force acting on the ejecta. Gopalswamy et al. (2001), on the other hand, proposed that all CMEs undergo constant acceleration (or deceleration) out to some fixed distance (0.76 AU) at which point they travel at constant speed. The simplest profile, of course, is to assume that a fast CME decelerates at a constant rate from the Sun to the point of observation at 1 AU (Gopalswamy et al. 2000). (The refinement of the Gopalswamy et al. (2000) result by Gopalswamy et al. (2001) was driven primarily by the fact that slow ICMEs seem to have a fairly constant arrival time (4.2 days). Thus it is not clear that such a profile is more appropriate to use here). It should be noted that all three acceleration profiles lead to predicted arrival times with the same average error (Owens & Cargill 2004). Thus, we will derive an expression for τ assuming constant deceleration. If an object move a distance d in time τ under constant acceleration from a speed of v_{c1} to v_{c2}, then:

$$\frac{d}{\tau} = \frac{v_{c1} + v_{c2}}{2} \tag{24}$$

From this, we can compute the transit time of the ICME:

$$\tau = \frac{2d}{v_{c1} + v_{c2}} \tag{25}$$

As an example, consider the 11/22/01 CME event analyzed in the previous section. From the in situ observations, we computed $v_{c2} = 800$ km/s, and from equation (23) we inferred $v_{c2} = 2152$ km/s. Using $d = 1$ AU, we estimate that $\tau = 28.2$ hours. This compares favorably with the value quoted in the literature (Reiner et al. 2007) of 31.0 hours. While the difference could be attributed to any number of reasons (and the difference is certainly within any error estimates that could be ascribed to either result), one potential factor is that the simple deceleration profile we used was not aggressive enough. The two-slope profile of Gopalswamy et al. (2001), for example, would likely have increased τ.

5. Summary and Discussion

n this study, we have used mass, momentum, and energy conservation to relate the properties of ICMEs observed in the solar wind to their coronal counterparts. In particular, assuming that both plasma and magnetic pressure could be neglected, in comparison to the dynamic (ram) pressure of the CME, we derived an estimate for the initial speed of the CME based on the observed in situ properties of the ejecta and its surroundings. We applied this relationship to a simulated CME, for which the true initial speed could be determined, to assess the accuracy of the technique. We found that the estimated speed for v_{c1} agreed with the actual speed to within $\sim 150/1400 \times 100\% \sim 10\%$, at least within the range of 0.5 - 2 AU. We also applied equation 23 to an event observed both at the Sun by LASCO/SOHO and in the solar wind by the Wind spacecraft. Using Wind measurements, we inferred v_{c1} to be 2151 km/s. This can be compared with speeds obtained from: (1) low-frequency radio emissions and transit times (Reiner et al. 2007), which yielded 2250 km/s; and (2) a "cone" model fit (Xue et al. 2005), which yielded 2519 . Generally, we have found that the radio and cone model techniques do not yield similar results. In fact, part of the motivation for choosing the November 22, 2001 event was that both techniques gave similar results. Thus, the technique developed here may potentially be used to resolve the disagreements between these two approaches, if it can be shown that two out of the three approaches produce similar estimates for v_{c1}.

Our derivation of equation (23) is replete with assumptions and approximations that, in some cases, cannot be rigorously defended. First, the system is treated as one-dimensional, i.e., spherically symmetric. For events where the ICME is intercepted at its flanks (i.e., a large impact parameter) or where substantial non-radial flows are observed, this approximation is not likely to be valid. Second, the ram pressure dominates over the thermal and magnetic pressures of the CME both close to the Sun and in the solar wind. Due to the spherical expansion of the solar wind, this approximation is almost certainly met in the solar wind; However, close to the Sun strong internal magnetic fields coupled with slower initial CME speeds may cast doubt on this approximation. If we restrict ourselves to distances sufficiently far from the Sun that non-radial expansion of the ejecta has ceased, say $20 - 30R_S$, this assumption likely holds to a first approximation. And third, the upstream solar wind speed remains constant and the upstream density varies by $1/r^2$. Eruption into a complex ambient solar wind structure may invalidate these assumptions. In spite of these significant approximations, we suggest that for fast CMEs equation (23) can serve as a useful tool in determining the initial speed of the CME. This is supported by our "numerical CME" experiment.

The accuracy and therefore potential usefulness of equation (23) can be assessed in a number of ways. First, by exploring the parameter space using 1-D simulations such as the one discussed here. The effects of spherical symmetry can be explored by using 3-dimensional MHD simulations of CME propagation and evolution, such as the Enlil model (Odstrcil et al. 2004), which can be run by the scientific community at the CCMC. In the case of Enlil, the initial properties of the CME close to the Sun can be prescribed using either arbitrary test values or results from a "cone model" fit to the white-light observations of the event. In either case, however, the intiial speed of the CME (v_{c1} is accurately known since it is an input into the model. These types of simulations can also be used to assess which technique (the one presented here, the cone model, and the radio technique) give the best estimate for the speed of the CME in the solar wind v_{c2} by running cases with each value of v_{c1} used to drive the model.

A significant limitation in the accuracy of equation (23) rests in the ratios of density, duration, and speed under the square root. These ratios either depend explicitly on the identified boundaries (i.e., the duration of the sheath and ICME) or implicitly through how the averages are made. For example, moving the boundary of the trailing edge of the ICME forward in time (i.e., making Δt_{c2} significantly larger) can change the estimated v_{c1} substantially. Often, different signatures suggest different locations: which one should be chosen? Since we are concerned with momentum transfer, we should generally chose the shorted interval that encompasses the bulk of the ejecta that is compressing the material ahead. Thus boundaries based on speed changes, density variations, magnetic field strength and rotation are likely to be more appropriate than boundaries based on counterstreaming suprathermals or composition variations. Our uncertainty in these boundaries can be used to estimate the errors associated with our calculation of v_{c1}, assuming that our approximations in the derivation of equation (23) did not introduce any large, systematic biases. In addition to choosing our best estimate of these boundaries, we could also chose several more extreme, yet still reasonable sets of boundaries and compute v_{c1} for each. The value with the largest deviation from our best estimate would provide an upper limit to the error.

In this study, we have outlined the derivation of some simple conservation relations and presented one specific application; to estimate v_{c1} for fast ICMEs. However, this technique could be modified to address the so-called "over-expanding" CMEs, which drive forward and reverse shocks ahead and behind them, respectively. Additionally, by retaining the thermal and magnetic pressure terms, inferences on the initial plasma-β of the CME could be made. These will be addressed in future studies.

PR gratefully acknowledges the support of the National Aeronautics and Space Administration (ST&T Program).

REFERENCES

Bothmer, V., & Schwenn, R. 1998, Annales Geophysicae, 16, 1

Burlaga, L. F. 1991, Magnetic Clouds. (Physics of the Inner Heliosphere II. Particles, Waves and Turbulence, XI, 352 pp. 152 figs.. Springer-Verlag Berlin Heidelberg New York. Also Physics and Chemistry in Space, volume 21; 2), 1–+

Burlaga, L. F., Sittler, E. C. J., Mariani, F., & Schwenn, R. 1981, J. Geophys. Res., 86, 6673

Forbes, T. G. 2000, J. Geophys. Res., 105, 23153

Gopalswamy, N., Lara, A., Lepping, R. P., Kaiser, M. L., Berdichevsky, D., & St. Cyr, O. C. 2000, Geophys. Res. Lett., 27, 145

Gopalswamy, N., Lara, A., Yashiro, S., Kaiser, M. L., & Howard, R. A. 2001, J. Geophys. Res., 106, 29207

Gosling, J. T., Bame, S. J., McComas, D. J., Phillips, J. L., Scime, E. E., Pizzo, V. J., Goldstein, B. E., & Balogh, A. 1994, Geophys. Res. Lett., 21, 237

Gosling, J. T., Hildner, E., MacQueen, R. M., Munro, R. H., Poland, A. I., & Ross, C. L. 1974, J. Geophys. Res., 79, 4581

Hu, Q., & Sonnerup, B. U. O. 2001, Geophys. Res. Lett., 28, 467

Klein, L. W., & Burlaga, L. F. 1982, J. Geophys. Res., 87, 613

Klimchuk, J. A. 2001, in in Space Weather Geophys. Monogr., Vol. 125 (Washington, DC: AGU), 143

Lepping, R. P., Jones, J. A., & Burlaga, L. F. 1990, J. Geophys. Res., 95, 11957

Lin, J., Soon, W., & Baliunas, S. L. 2003, New Astronomy Review, 47, 53

Low, B. C. 1994, Physics of Plasmas, 1, 1684

Marubashi, K. 1997, in Coronal Mass Ejections (Geophys. Monogr.), ed. N. U. Crooker, J. A. Joselyn, & J. Feynman, Vol. 99 (Washington, DC: AGU), 147

Odstrcil, D., Pizzo, V. J., Riley, P., & Arge, C. N. 2004, AGU Fall Meeting Abstracts, A1+

Owens, M., & Cargill, P. 2004, Annales Geophysicae, 22, 661

Reiner, M. J., Kaiser, M. L., & Bougeret, J.-L. 2007, Ap. J., 663, 1369

Riley, P., & Gosling, J. T. 1998, Geophys. Res. Lett., 25, 1529

Riley, P., Gosling, J. T., & Pizzo, V. J. 2001, J. Geophys. Res., 106, 8291

Rust, D. M. 1994, Geophys. Res. Lett., 21, 241

Sheeley, N. R., Walters, J. H., Wang, Y.-M., & Howard, R. A. 1999, J. Geophys. Res., 104, 24739

Tousey, R. 1973, BAAS, 5, 419

Vršnak, B., & Gopalswamy, N. 2002, J. Geophys. Res, 107, 1019

Wu, S. T., Guo, W. P., Michels, D. J., & Burlaga, L. F. 1999, J. Geophys. Res., 104, 14789

Xue, X. H., Wang, C. B., & Dou, X. K. 2005, J. Geophys. Res., 110, 8103

Zhao, X. P., Plunkett, S. P., & Liu, W. 2002, J. Geophys. Res., 13

Zurbuchen, T. H., & Richardson, I. G. 2006, Space Science Reviews, 123, 31

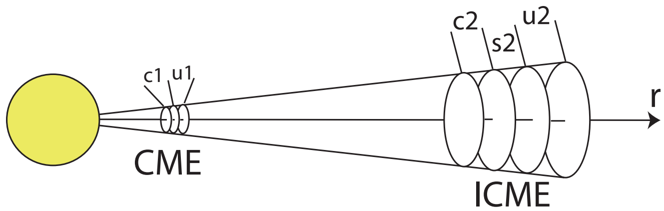

Fig. 1.— Illustration of the two regions of space under study. The location of the CME, close to the Sun is referred to region 1 and covers the spatial range denoted be c1. The material upstream, which will eventually be swept up into sheath material is denoted u1. In the solar wind, the location of the ICME is referred to as region 2 and covers the spatial range c2. The sheath region is denoted by s2 and the region upstream of the entire disturbance is denoted by u2.

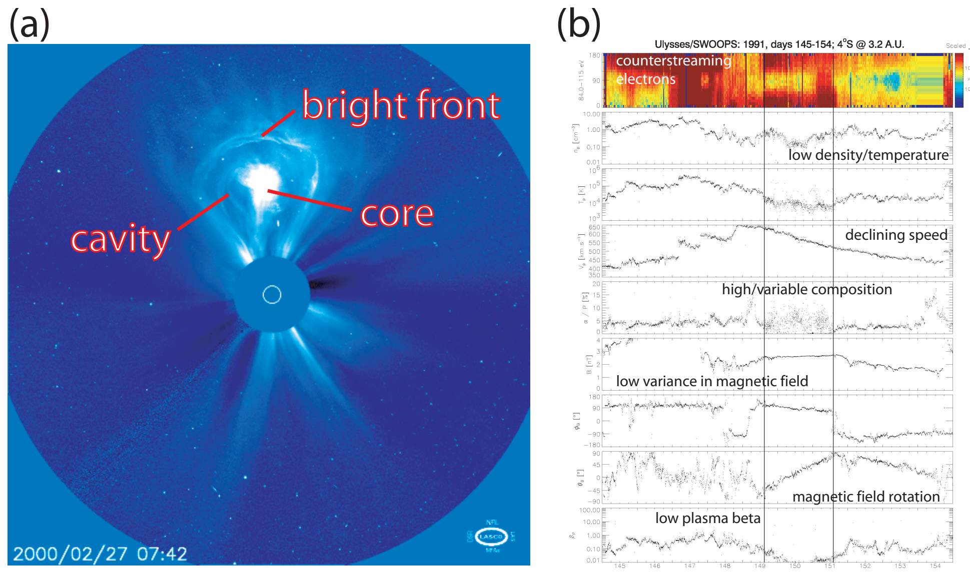

Fig. 2.— (a) An example of a classic 3-part CME, with the core, cavity, and bright front marked. (b) An example of an ICME displaying many "classic" signatures, as indicated.

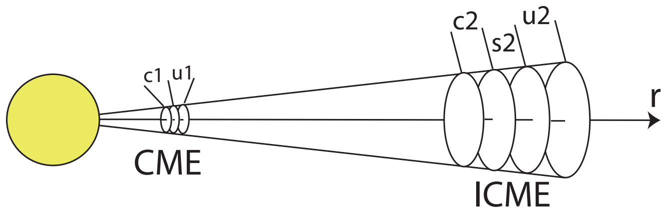

Fig. 3.— Illustration of the two regions of space under study. The location of the CME, close to the Sun is referred to region 1 and covers the spatial range denoted be c1. The material upstream, which will eventually be swept up into sheath material is denoted u1. In the solar wind, the location of the ICME is referred to as region 2 and covers the spatial range c2. The sheath region is denoted by s2 and the region upstream of the entire disturbance is denoted by u2.

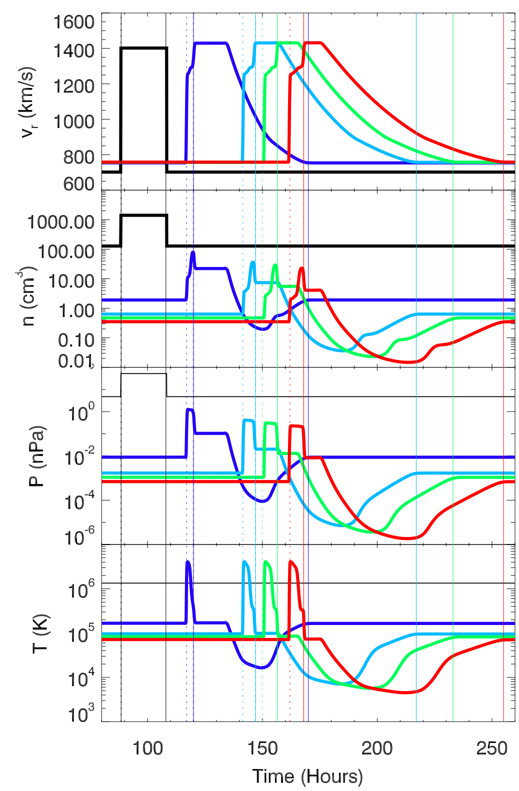

Fig. 4.— Time series of: Speed (v); number density (n); pressure (P), and temperature (T). In each panel, time profiles are shown from 5 locations: 0.14 AU (black), 0.5 AU (dark blue), 1.0 AU (light blue), 1.5 (green), and 2.0 AU (red). The inner boundary of the simulation was located at 0.14 AU, and thus the black profiles summarize the initial perturbation, mimicking the CME. In this case, it consisted of a speed jump of 700 km/s with a coincident density enhancement of one order of magnitude. The location of the CME-driven shock for each time profile is marked by the dotted line while the boundary of the ejecta is marked by two solid lines of the appropriate color.

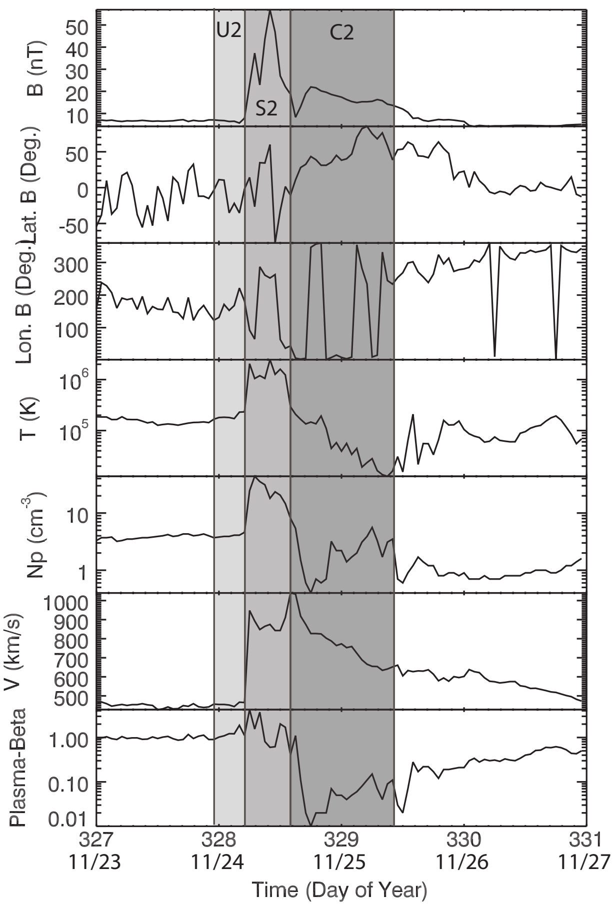

Fig. 5.— Time series of: field magnitude (B), the latitude and longitude angles of B, the plasma temperature (T), the plasma number density (Np), the plasma bulk flow speed (V), and the plasma-beta at 1 AU for the November 22, 2001 CME. Data from the OMNI data archive.

Table 1: Computation of v_{c1} for 1-D hydrodynamic simulation.

Parameter	0.5 AU	1.0 AU	1.5 AU	2.0 AU
vc2	1105	1051	1047	1047
dtc2	50.0	70.0	76.5	87.0
nc2	7.90	1.45	0.941	0.600
vu2	754	754	754	754
vs2	1271	1280	1213	1281
dts2	3.0	5.5	6.5	6.0
ns2	32.6	13.6	9.58	8.70
dts2/dtc2	0.060	0.0786	0.0850	0.0690
ns2/nc2	4.13	9.40	10.2	14.5
vs2/vc2	1.15	1.22	1.16	1.22
SQRT($vs2^2 - vu2^2$)	1023	951	1035	1035
VC1	1232	1438	1415	1551

7. Appendix C

Global MHD Modeling of the Solar Wind and CMEs: Energetic Particle Applications

Pete Riley, Jon A. Linker, Zoran Mikic, and Roberto Lionello

Published in the *AIP Conference Proceedings*, September, 2008.

Global MHD Modeling of the Solar Wind and CMEs: Energetic Particle Applications

Pete Riley, Jon A. Linker, Zoran Mikic, and Roberto Lionello

Science Applications International Corporation, San Diego, California.

Abstract. Global MHD models of Coronal Mass Ejections (CMEs) can provide important insights into the physical processes associated with the eruption and evolution of CMEs and the acceleration of SEPs, and are a valuable tool for interpreting both remote solar and interplanetary in situ observations. Moreover, they represent a virtual laboratory for exploring conditions and regions of space that are not conveniently or currently accessible by spacecraft. The most energetic events typically originate from active regions on the Sun. To accurately model such regions, whilst also capturing the global corona, requires an MHD model that includes energy transport (radiative losses, anisotropic thermal conduction, and coronal heating) in the transition region and corona. Equally importantly, the model must reproduce an accurate ambient solar wind through which the CME propagates. In this report, we describe the current status of modeling efforts, and present three applications that we believe are relevant in studies of energetic particles: the Alfvén speed in the corona; the evolution of the heliospheric current sheet; and CME eruptions.

Keywords: Global MHD Model, Coronal Mass Ejections, Corona, Solar Wind, Coronal Heating, EIT Waves, Dimming Regions, Post-Flare Loops
PACS: 96.60.ph, 96.60.P-, 96.60.Q-, 96.60.qd, 96.60.Vg

INTRODUCTION

With advances in computing capabilities and resources, the development of parallel programming paradigms, improvements in numerical techniques, and a better understanding of coronal physics, global MHD models are reaching the point where they can make meaningful contributions toward understanding a variety of fundamental problems associated with the acceleration and transport of energetic particles.

In this report we summarize the current status of our global, time-dependent MHD modeling efforts at SAIC, and in particular, describe three topics that may be of broad relevance to the energetic particle physics community. Complementary studies by teams at the University of Michigan [1] and the University of Hawaii [2] are also reported in these proceedings.

THE SAIC MHD MODEL

SAIC's global coronal and heliospheric code (MAS) solves the usual set of time-dependent, resistive MHD equations in spherical coordinates [3]. These equations are solved on nonuniform meshes, which allows us to concentrate grid points in regions of interest. The method of solution, including the boundary conditions, has been described previously [3, 4, 5, 6, 7, 8]. Here we restrict our discussion to some comments concerning how energy transport processes are treated. We write the energy equation as:

$$\frac{1}{\gamma-1}\left(\frac{\partial T}{\partial t}+\mathbf{v}\cdot\nabla T\right)=-\,T\nabla\cdot\mathbf{v}+S, \tag{1}$$

where

$$S=\frac{1}{2kn_e}\left(-\nabla\cdot\mathbf{q}-n_e n_p Q(T)+H+H_d+D\right), \tag{2}$$

$\mathbf{v}$ is the plasma velocity, T is the plasma temperature, n_p and n_e are the proton and electron densities, respectively, k is the Boltzmann constant, H is the coronal heating source, $H_d=\eta J^2+\nu\nabla\mathbf{v}{:}\nabla\mathbf{v}$ is the heating due to resistive and viscous dissipation, D is the heating due to dissipation of Alfvén waves, and $Q(T)$ is the radiation loss function [e.g., 9]. In the collisional regime (below $\sim 10R_s$), the heat flux is given by $\mathbf{q}=-\kappa_{\|}\hat{\mathbf{b}}\hat{\mathbf{b}}\cdot\nabla T$, where $\hat{\mathbf{b}}$ is the unit vector along $\mathbf{B}$, and $\kappa_{\|}=9\times10^{-7}T^{5/2}$ is the Spitzer value of the parallel thermal conductivity (in cgs units). In the collisionless regime (beyond $\sim 10R_s$), the heat flux is given by $\mathbf{q}=\alpha n_e kT\mathbf{v}$, where α is a dimensionless parameter of order 1 [10]. Although the (unknown) coronal heating source H is a parameterized function, Lionello et al. [11] have described how we can evaluate different coronal heating models by comparing simulated EUV and X-ray emission with observations.

Ambient solutions are produced by integrating the equations forward in time until a steady state is achieved. Simulations of CME eruptions are produced by applying time-dependent changes to the boundary conditions of a steady-state solution. Previously, we have studied the possibility that eruptions could be initiated by photospheric motions that shear and twist the coronal magnetic field [12, 13, 4, 3]. These results show that when the magnetic field is azimuthally sheared beyond a critical value, helmet streamer configurations can erupt in a manner similar to observed “slow" CMEs. A more promising mechanism for producing fast CMEs is magnetic flux cancellation [14, 7].

THE ALVÉN SPEED IN THE SOLAR CORONA

For our first application, we consider the variation of MHD wave speeds in the solar corona and what they imply for the generation of coronal shocks. For simplicity we focus on the Alfven speed; however, this analysis could be undertaken with the fast-mode speed too, given some assumptions about the direction of the field.

As an illustration, we summarize the structure of the corona surrounding the January 20, 2005 CME, which has been the topic of several talks at this conference, and is, arguably, the most spectacular event of the Space Age. Figure 1(a) shows a slice of the computed Alfvén speed in the equatorial plane based on a thermodynamic model of the time period. The vertical line from the center of the Sun upwards marks the location of active region (AR) 720, which was the inferred source of the CME. It is important to emphasize that these speeds could not have been computed reliably using the simpler polytropic formulation, where the user is free to set the density at the base of the corona and hence ‘tune’ the Alfvén speed to any value desired. In the thermodynamic model, density and temperature are no longer free parameters. Instead, parameters associated with the heating of the corona are chosen (constrained by comparisons of simulated and

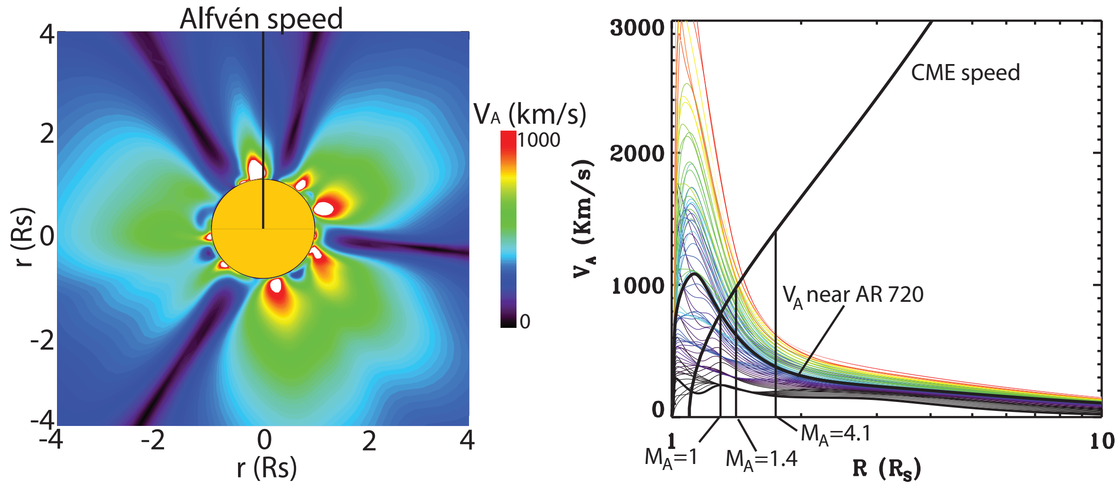

FIGURE 1. *(a) Computed Alfvén speed in the equatorial plane. (b) A selection of Alfvén speed profiles surrounding AR 720. One is chosen for emphasis. Also shown is the speed of the CME as inferred from SOHO observations. The vertical lines mark points along the CME's trajectory when values of M_A = 1, 1.4, and 4.1 are reached.*

observed emission, which depends sensitively on the heating parameters) and the plasma properties are a product of the calculation.

Figure 1(b) shows the Alfvén speed versus height for a selection of radial traces surrounding the AR: There is significant variation in Alfvén speed, depending on position relative to the center of the AR. The thick solid line emanates from a point nearby the AR and represents, in some sense, an average of these traces. Comparing this with the inferred CME speed derived from SOHO observations [15] shows that shock formation ($M_A > 1$) was certainly possible by $1.2 - 1.4 R_S$ [1]. To accelerate electrons sufficiently to produce type II radio emission requires an Alfvén Mach number of at least 1.4 [17, 18] - and may also depend crucially on geometry - which occurs not much further out; perhaps a few 10ths of a solar radii. Following the accelerating CME further out, the medium into which it propagates presents a decreasing Alfvén speed profile and a super-critical shock is reached when the Mach number exceeds 4.1. At that point, the shock can accelerate both electrons and ions efficiently. All of this occurs within 1.7 Rs. In terms of timing: the CME becomes super-Alfvénic within 3 minutes; type II radio emission occurs in less than 5 minutes; and the shock becomes supercritical within 10 minutes.

[1] At the workshop, J. R. Jokipii raised the interesting point that the flow need not be super-Alfvénic for a shock to form. He cited the 1-D shock tube as an example [16]. While this is certainly true for configurations where there is no possibility for the flow to escape around an object (or driver), it is not clear how relevant it is to the formation of shocks in the corona, where the CME driving the shock is a blunt object. Jokipii (personal communication, 2008) suggested that locally, the nose of the driver front is essentially flat. Thus it is possible that, at least on a very local scale (and over some as yet to be determined transient time) a shock would form prior to the condition $M_A = 1$ being reached. Whether this would have any practical effect on the acceleration of particles is, however, remains questionable. Nevertheless it is something that has not been considered previously, and, until it is more thoroughly studied, care should be taken when inferring shock formation based solely on Mach number.

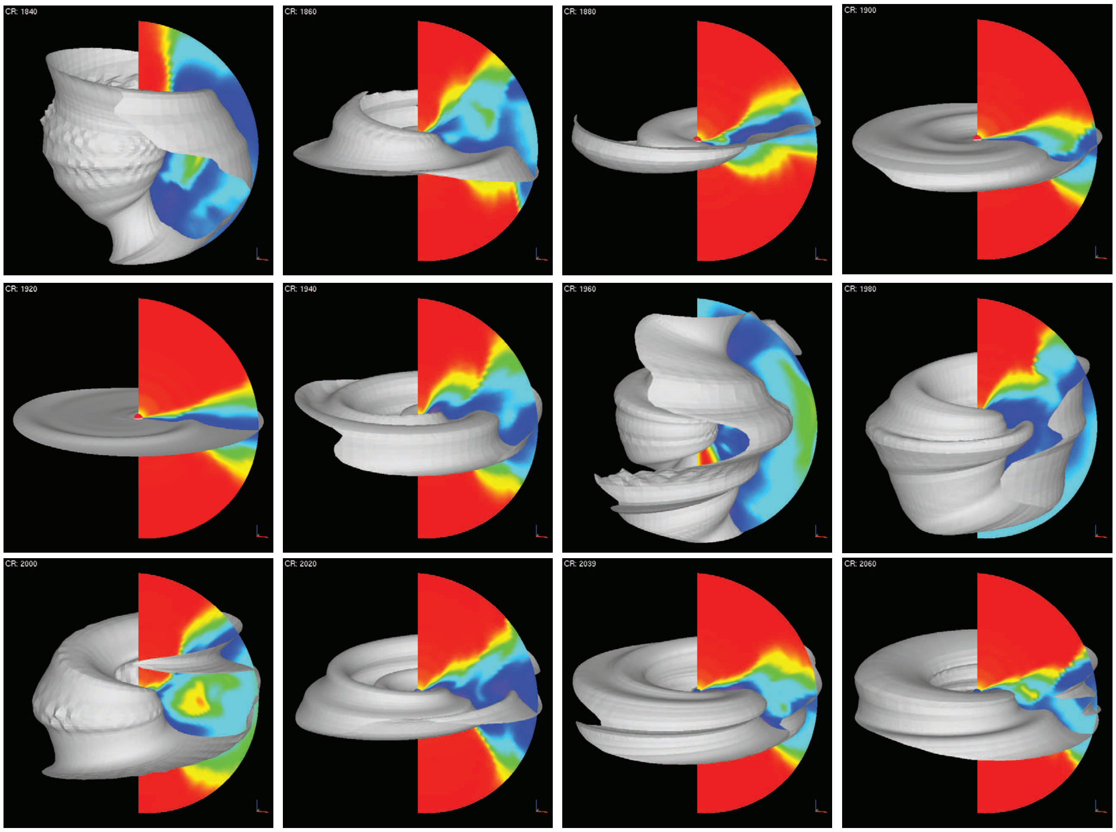

FIGURE 2. *Evolution of the HCS from Carrington Rotation 1840 through 2060, roughly corresponding to the duration of the Ulysses mission. The slice in the meridional plane shows the radial velocity at that longitude. Each frame is separated by 20 Carrington rotations (or* ~ 1.4 *years).*

Finally, we remark that shock formation and evolution will proceed quite differently along different radial trajectories. Figure 1(a) suggests that a longitudinally-extended pressure wave propagating away from the Sun above AR 720 will shock first on its flanks and then above the AR. Extrapolating to three dimensions, the shock might form first as an annulus around the AR.

THE HELIOSPHERIC CURRENT SHEET

As a second example of how the MHD models might be useful for energetic particle applications we draw attention to studies we have performed to understand the structure and evolution of the heliospheric current sheet (HCS) [19]. Current models of galactic cosmic ray modulation rely on a simplified description of the HCS, treating it simply as a wavy structure and retaining information only about its tilt angle [20]. As particle transport models become more sophisticated in the future, it may be possible to incorporate a more detailed description of the HCS, based on MHD solutions, such as those presented here.

As the Ulysses mission draws to an end, it is fitting for us to illustrate the evolution of the HCS over the last 17.5 years. Figure 2 attempts to do this. Each frame is separated by 20 Carrington rotations, and together, they capture the second half of solar cycle 22 and the entirety of solar cycle 23. These changes can be seen in: the latitudinal extent of the HCS; the complexity of the radial velocity; and the latitudinal extent of the fast solar wind.

CME ERUPTIONS: COMPARISONS WITH OBSERVATIONS

For our last application, we consider features associated with the eruption of CMEs. We use the May 12, 1997 CME event for illustration. The simulation results have been described in detail by Linker et al. [21], who include a discussion of the formation of a sigmoid structure, dimming regions, and post-flare loops. For the purposes of brevity, we focus on one specific aspect of the event, namely, the generation and propagation of the EIT waves.

For many years it had been thought that EIT waves were fast-mode waves propagating horizontally in the low corona. Recently, several groups have challenged this idea [22, 23], motivated, at least in part, by the apparent discrepancy between the observed wave speed and that computed from estimates of the density and magnetic field strength in the corona as well as from simplified polytropic models. Here, we demonstrate that our thermodynamic solutions match the EIT wave speeds remarkably well.

In Figure 3(a) are a sequence of images from EIT of the May 1997 event. The speed of the perturbation was computed to be 245 km s^{-1} [24]. Simulated EIT difference images showing the propagation of similar-looking disturbances are shown in Figure 3(b). By tracking the motion of pressure fronts along various trajectories away from the AR and across the disk, we can compute the speed of the simulated EIT wave. Figure 3(c) compares the results of this analysis with the computed slow, Alfvén, and fast waves along the same trajectory. Thus we find that the computed speeds are fully consistent with the fast-mode speed. Moreover, the model predicts a speed of between 270 and 340 km s^{-1}, which is (to within error estimates) consistent with the observed speed of 245 km s^{-1}. Finally, we note that pressure and field strength perturbations are in phase, which would be expected for a fast-mode wave.

SUMMARY

In summary, global MHD simulations have now reached a level of sophistication that we can study specific events in detail and make meaningful comparisons with observations. These solutions provide a unique way to understand a range of complex physical phenomena, occurring at, and away from the Sun. In this report, we have provided three examples of how the MHD results may contribute to our understanding of energetic particle physics. However, this application is clearly still in its infancy.

NASA (SR&T and SECT programs) and NSF (SHINE and CISM programs) supported the work presented here.

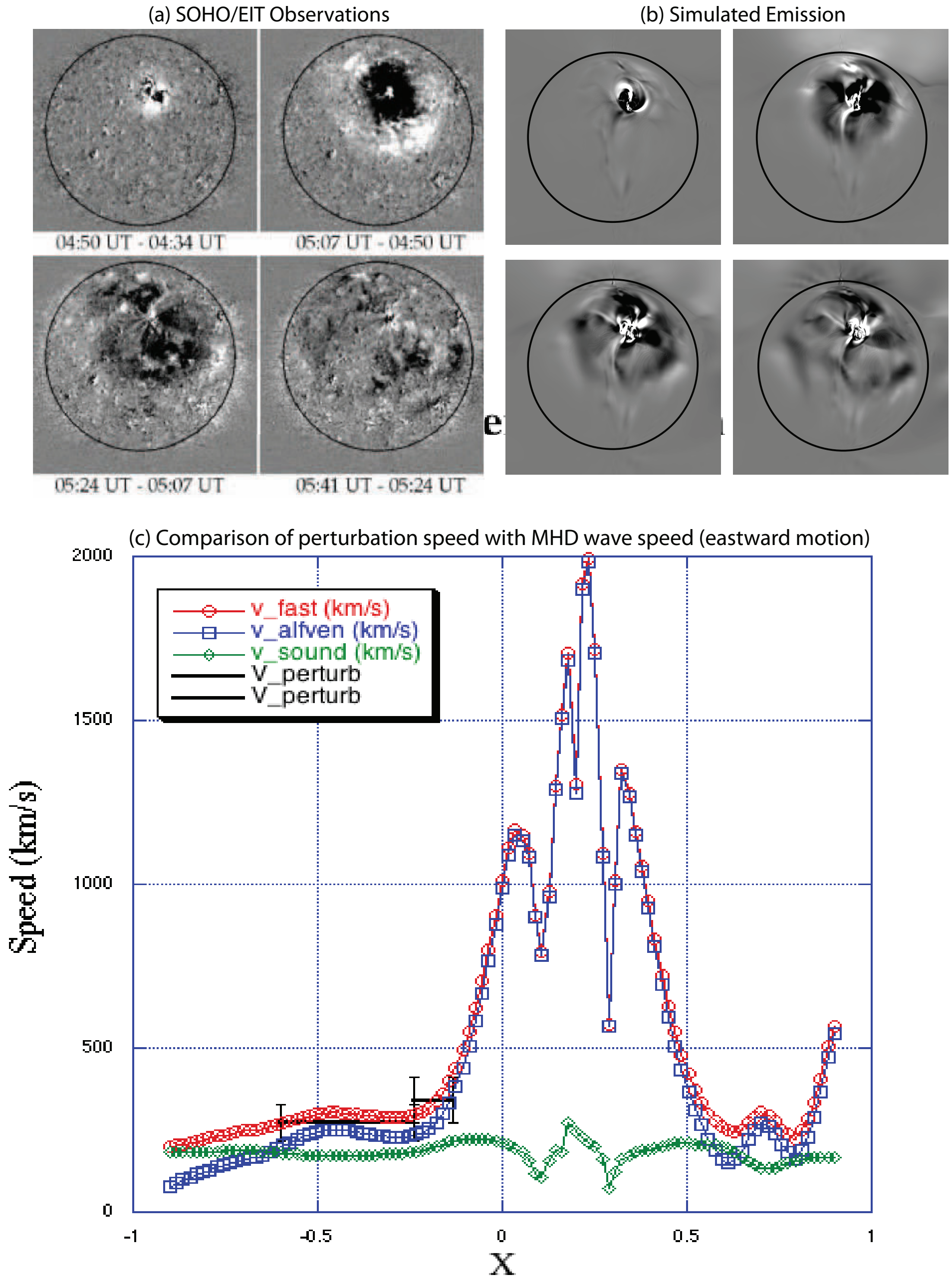

FIGURE 3. *(a) and (b): Comparison of the observed EIT wave with the wave produced in the MHD simulation. (c) Comparison of the computed MHD wave speeds with the speed of the perturbation.*

REFERENCES

1. W. B. Manchester IV, G. Toth, I. Sokolov, T. H. Zurbuchen, and J. Kota, "MHD Simulations of CME-Driven Shocks: Structures Relevant to Particle Acceleration," in *7th IGPP/SSL Astrophysics Conference*, American Institute of Physics Conference Series, this volume, 2008.

2. I. Roussev, N. Lugaz, and I. Sokolov, “Global MHD Modeling of CMEs and Related Shocks from Complex Active Regions,” in *7th IGPP/SSL Astrophysics Conference*, American Institute of Physics Conference Series, this volume, 2008.
3. Z. Mikić, and J. A. Linker, *ApJ* **430**, 898 (1994).
4. J. A. Linker, and Z. Mikić, *Coronal Mass Ejections* **99**, 269 (1997), edited by N. Crooker, J. Joselyn, and J. Feynmann, p. 269, AGU, Washington, D. C.
5. R. Lionello, Z. Mikić, and J. A. Linker, *J. Comp. Phys.* **152**, 346 (1999).
6. Z. Mikić, J. A. Linker, D. D. Schnack, R. Lionello, and A. Tarditi, *Phys. Plasmas* **6**, 2217 (1999).
7. J. A. Linker, R. Lionello, Z. Mikić, and T. Amari, *J. Geophys. Res.* **106**, 25165 (2001).
8. R. Lionello, J. A. Linker, and Z. Mikić, *ApJ* **546**, 542 (2001).
9. R. Rosner, W. H. Tucker, and G. S. Vaiana, *Ap. J.* **220**, 643–645 (1978).
10. J. V. Hollweg, *Reviews of Geophysics and Space Physics* **16**, 689–720 (1978).
11. R. Lionello, J. A. Linker, and Z. Mikic, “The Multispectral Emission of the Sun during August 1996,” in *American Astronomical Society Meeting Abstracts*, 2007, vol. 210 of *American Astronomical Society Meeting Abstracts*, pp. #91.08–+.
12. Z. Mikić, D. C. Barnes, and D. D. Schnack, *ApJ* **328**, 830 (1988).
13. J. A. Linker, and Z. Mikić, *Ap. J. Lett.* **438**, L45 (1995).
14. T. Amari, T. Boulmezaoud, and Z. Mikić, *Astron. Astrophys.* **350**, 1051 (1999).
15. N. Gopalswamy, S. Yashiro, Y. Liu, G. Michalek, A. Vourlidas, M. L. Kaiser, and R. A. Howard, *J. Geophys. Res.* **110**, 9–+ (2005).
16. L. D. Landau, and E. M. Lifshitz, *Fluid mechanics*, Course of theoretical physics, Oxford: Pergamon Press, 1959, 1959.
17. G. Mann, A. Klassen, H. Aurass, and H. T. Classen, “Development of shocks waves in the solar corona and the interplanetary space,” in *AIP Conf. Proc. 679: Solar Wind Ten*, 2003, pp. 612–615.
18. G. Mann, A. Klassen, H. Aurass, and H.-T. Classen, *Astron. Astrophys.* **400**, 329–336 (2003).
19. P. Riley, J. A. Linker, and Z. Mikić, *J. Geophys. Res.* **107**, DOI 10.1029/2001JA000299 (2002).
20. J. Kota, and J. R. Jokipii, “Cosmic ray effects of the global magnetic field in the inner and outer heliosphere,” in *35th COSPAR Scientific Assembly*, 2004, vol. 35 of *COSPAR, Plenary Meeting*, pp. 3859–+.
21. J. A. Linker, Z. Mikic, R. Lionello, P. Riley, and V. Titov, “EIT Waves in an MHD Simulation of the May 12, 1997 CME,” in *Invited talk presented at the 2007 SHINE Workshop*, 2007.
22. G. D. R. Attrill, L. K. Harra, L. van Driel-Gesztelyi, and P. Démoulin, *Ap. J. Lett.* **656**, L101–L104 (2007).
23. M. J. Wills-Davey, C. E. DeForest, and J. O. Stenflo, *Ap. J.* **664**, 556–562 (2007).
24. B. J. Thompson, S. P. Plunkett, J. B. Gurman, J. S. Newmark, O. C. St. Cyr, and D. J. Michels, *Geophys. Res. Lett.* **25**, 2465–2468 (1998).